Journal name: Ecological Applications

Manuscript type: Article

Manuscript title: **Playing it safe at early life stages: Balancing energy allocations to maximize fitness under seasonal pathogen dynamics**

Authors: Zuania Colón-Piñeiro[1], Nich W. Martin[2], Travis J Klee[1], Brittaney L Buchanan[1], Colette M St. Mary[1,3], Miguel A. Acevedo[4], Patricia Burrowes[5,6], and Ana V. Longo[1]

Affiliations: [1]Department of Biology, University of Florida, [2]Department of Entomology and Nematology, University of Florida, [3]National Science Foundation, [4]Department of Wildlife Ecology and Conservation, University of Florida, [5]Department of Biology, University of Puerto Rico, [6]National Museum of Natural History, Madrid, Spain.

Corresponding author: **Zuania Colón-Piñeiro**, email zcolonp@gmail.com, phone (939)633-4705, address 421 Carr Hall 876 Newell Dr. University of Florida Gainesville, FL 3261; **Ana V Longo**, email: ana.longo@ufl.edu, phone (352)214-0882, address 421 Carr Hall 876 Newell Dr. University of Florida Gainesville, FL 3261.

Open Research statement: Script developed to generate model solution, forward iterations, and the sensitivity analysis, as well as figures, is available during review in a private link from FigShare, https://figshare.com/s/8be08deca455559725a4, and will be publicly available after publication.

Keywords: direct-developing amphibians; dynamic state variable model; energetic constraints; host-pathogen interactions; tradeoffs; seasonality in the tropics.

Abstract

Immune responses are crucial in controlling diseases and maintaining host homeostasis, but they involve inherent tradeoffs due to the competing demands for resource allocation among physiological processes. While energy allocation tradeoffs shape individual phenotypes, they are rarely included in disease ecology models. Environmental factors like limited food availability and adverse climates decrease individual fitness by increasing pathogen virulence and host susceptibility. Despite that seasonal resource availability affects competition among physiological processes, research has mostly focused on the pathogen dynamics rather than on the trajectories of hosts under varying resource availability scenarios. Here, we implemented dynamic optimization state models to determine which changes in energy allocation maximize fitness in amphibians with enzootic infections —when the pathogen consistently infects the population—. We hypothesized that young individuals allocate energy for growth at lower infection levels but shift to immunity as pathogen-mediated damage increases. We predicted that shifts in energy allocation result in lower fitness, measured as size, time to maturity, and survival. We also expected that the season at which individuals are born exacerbates these tradeoffs, increasing fitness variability within the population. Based on our models, we identified critical windows that maximize individual growth while limiting mortality under increased pathogen burden. The models highlighted that seasonality in pathogen exposure and foraging success exacerbates growth-defense tradeoffs, leading to delayed maturity and lower survival rates when frogs hatch under sub-optimal environmental conditions. Our simulations support empirical results, showing that increased frog reproduction coincides with high resource availability and low pathogen risk. Our findings demonstrate that shifts in energy allocation affect population size and recruitment, modulate

prevalence and infection intensity, and constrain fitness traits. We highlight the utility of dynamic state variable models in examining how host fitness strategies impact early-life growth rates and population survival under varying seasonal and resource conditions, providing a framework to understand the outcomes of emerging diseases under predicted climate change scenarios. The flexibility of using generic units allows ecologists to apply the findings to different contexts, such as extreme droughts, pathogen outbreaks, or species reintroduction programs, by adjusting parameter values based on empirical data from experiments and field observations.

Introduction

Immune responses are one of the most critical factors in controlling diseases and maintaining homeostasis in the host. While empirical studies show that energy allocation tradeoffs affect growth, survival, and reproduction, individual fitness is rarely included in disease ecology models. Infections can determine the fate of individuals, and the activation of the immune system in non-lethal cases comes with an energetic cost, resulting in a tradeoff between immunity and other physiological processes (Brannelly *et al.* 2021a; Keehnen *et al.* 2021; Soler *et al.* 2003). Infected individuals often reduce their energy investment in development (Keehnen *et al.* 2021), growth (Korfel *et al.* 2015; Soler *et al.* 2003), and reproduction (Brannelly *et al.* 2021a; French *et al.* 2007), likely mediating the arms race with pathogen virulence. Despite that the tradeoffs in energy due to competition among these physiological processes affect the fate of individuals, research has primarily focused on the dynamics of the pathogen (Dwyer *et al.* 1997; Fleming-Davies *et al.* 2015) rather than on the trajectories of individuals under varying resource availability scenarios.

Life history theory predicts that early-life resource allocation strategies will determine future fitness by influencing the state —phenotype— of an individual at maturity (McNamara & Houston 1986; Stearns 2000). Larger body size at maturity results in higher fecundity (Stearns 2000) and size of the offspring (Hall *et al.* 2020; Townsend & Stewart 1994), thus enhancing fitness. Pathogen exposure at early life stages can have negative carryover effects on survival by affecting condition-dependent traits like growth, even after individuals successfully clear infections (Burrowes *et al.* 2008; Garner *et al.* 2009; Rumschlag & Boone 2020; Taborsky 2006). Although tradeoffs between energy-demanding processes have been widely studied across taxa (Brannelly *et al.* 2021b; Grogan *et al.* 2020; Huot *et al.* 2014; Keehnen *et al.* 2021), their

interactions vary across scales and intensify under sub-optimal conditions for the host, such as limited food availability and adverse environmental factors (Altizer *et al.* 2006; Civitello *et al.* 2018; Cressler *et al.* 2014). To assess the consequences of infections on individual fitness, it is essential to quantify how infection constrain energy-demanding processes like growth at early life history stages.

Pathogen virulence, host exposure, susceptibility, and infection are often mediated by environmental conditions such as seasonality (Andreasen & Dwyer 2023; Longo *et al.* 2010), making seasonal outbreaks a pervasive challenge across animal and plant communities (Altizer *et al.* 2006). Changes in abiotic conditions modulate host-pathogen interactions by altering host behavior, contact rates among individuals, births, and deaths in the population (Altizer *et al.* 2006; Civitello *et al.* 2018). Abiotic conditions also affect the ability of hosts to mount immune responses (Le Sage *et al.* 2021) and the recruitment of beneficial symbionts from the environment (Altizer *et al.* 2006; Longo *et al.* 2015; Nelson 2004). Most of these factors are driven by shifts in resource availability (Rumschlag & Boone 2020; Stewart & Woolbright 1996) and foraging success (Alvarado-Rybak & Azat 2021; Rumschlag & Boone 2020) between seasons. Understanding the fitness consequences of these tradeoffs is particularly important given the global rise of emerging and re-emerging diseases due to climate change (El-Sayed & Kamel 2020).

The patterns and processes that mediate tradeoffs in disease ecology vary by level of organization. At the population, susceptible and infected models predict pathogen spread based on individual abundance (Alizon *et al.* 2009; DiRenzo *et al.* 2019; Drewry 1970; Dushoff 1999; Miller *et al.* 2005; Simon *et al.* 2022; Stephenson *et al.* 2017), often assuming homogeneous populations and ignoring sources of variability (but see, Dwyer *et al.* 1997;

Fleming-Davies *et al.* 2015; Simon *et al.* 2022). For example, age structure can stabilize a population after an outbreak (Simon *et al.* 2022). At the individual, predator-prey models evaluate competition for limited resources like energy. Tradeoffs in energy allocation between host metabolism, immune cells, and pathogens lead to different outcomes depending on the scenario (Civitello *et al.* 2018; Cressler *et al.* 2014). For example, in high-resource scenarios, vertebrate hosts invest in immunity (Cressler *et al.* 2014), while parasites exploit these resources to mediate host immune cells by stealing energy (Graham 2008; Ramesh & Hall 2023). Therefore, theoretical models should incorporate heterogeneity in susceptibility among individuals (Dwyer *et al.* 1997).

Here, we develop mathematical models to identify strategies that increase host fitness when infected with endemic pathogens —where pathogens are consistently present in the host population— and how seasonality mediates host-pathogen dynamics. This modeling framework will allow us to understand how the interaction between the level of infection (*i.e.*, pathogen burden) and local seasonality (*i.e.*, differences in resource availability and infection probability) mediates host growth rates at early life stages (Fig. 1a) and how plasticity in energy allocation affects population survival. Dynamic optimization models can identify the optimal defense strategy that minimizes the cost of infection at the individual level (Shudo & Iwasa 2004). These models, built on the underlying process of the observed relationships, allow us to describe hypotheses quantitatively and generate predictions for testing on empirical settings (Mangel & Clark 1988; McCauley *et al.* 2000).

Using the well-studied *Eleutherodactylus coqui-Batrachochytrium dendrobatidis* (*Bd*) as the host-pathogen study system (Box1), we parameterized an agent-based models to evaluate how the growth-immune tradeoff in energy allocation at early life stages affects fitness. First, we

identified the set of host strategies across one year that maximize future fitness. We hypothesized that the optimal strategy for young individuals is to allocate energy for growth at lower infection levels but shift energy to immune defenses as pathogen-mediated damage increases. We then tracked simulated individuals using these energy allocation strategies, hypothesizing that lower growth rates of infected individuals result from energy shifts to immune defense (*i.e.*, control infection), while higher growth rates allow rapid reproductive maturation if the level of infection is manageable (Fig. 1b). Next, we evaluated whether seasonal shifts in resource availability and pathogen exposure exacerbated these tradeoffs (Fig. 1b), expecting smaller individuals, longer times to maturity, and increased mortality in cohorts born during less conducive growth conditions. Finally, we assessed the fate of the cohort by analyzing individual trajectories throughout the year. Our findings provide a modeling framework to quantify mismatches in reproductive activity, food availability, and differing infection exposure within a seasonal context. This model can be adapted to different taxa and climatic scenarios by varying season lengths, order, and parameter values.

Methods

Dynamic optimization models are used to study physiological tradeoffs by identifying strategies that maximize individual fitness (Mangel & Clark 1988). This process involves three steps: 1. Programing a stochastic dynamic equation to define changes in state variables over time, 2. Identifying strategies that optimize future fitness using backward interactions 3. Tracking individual trajectories over time by running forward iterations where virtual individuals select strategies that increase the expected fitness state based on resource availability and risk of mortality (Clark & Mangel 2000).

Within this model approach, we developed two dynamic state variable models to determine the energy allocation pattern that maximizes the host's future fitness. Note that we use survival and body size as a proxy for future fitness under pathogen infection because larger body size implies higher survival (Cabrera-Guzmán *et al.* 2013; Székely *et al.* 2020), higher fecundity (Stearns 2000), and more (Townsend & Stewart 1994) or larger offspring (Hall *et al.* 2020). Although we did not directly include reproduction in the model, the energy invested in reproduction was accounted for by decreasing the growth rate by size unit in adults (see below). We estimated the expected future fitness at the end of our time horizon: one year. The discrete state variables of interest in our models were time (t), size (S), and level of infection (I). Given that not all individuals have the same fate within a population, we incorporated individual heterogeneity through the following probabilities: available energy obtained by foraging (E), an uninfected individual becoming infected (P_I), and the probability of dying from natural causes as a function of body size ($M_S(S)$) and due to the level of infection ($M_I(I)$). In the basic model, these parameter values were constant across time. In the seasonal model, the probabilities of obtaining energy (E) and of becoming infected (P_I) depended on the season (Warm/Cool). This set of generic units for variables and parameters can be applied to multiple scenarios across taxa, but their values must be relative to the specific system that is been studied (Breckling 2002; Mangel & Clark 1988).

We used available field data on the host *Eleutherodactylus coqui* and the pathogen *Batrachochytrium dendrobatidis* (*Bd*) to parameterize a two-season model (Box 1, Table 1). The host is a terrestrial species that reproduces all year round; its life history and the host-pathogen dynamic with *Bd* have been well characterized among seasons in nature and laboratory experiments (Box 1). We modeled frog energy allocation when faced with

Bd-infection during development as juveniles, starting with hatching from the egg. Specifically, we identified the state-dependent allocation to growth and immune function that maximized the expected future reproductive success at the end of the time horizon. Then, with the predicted frog energy allocations that maximize future fitness, we implemented an individual-based model to simulate populations of individuals using these optimal strategies to describe the growth trajectories (Breckling 2002; Graham *et al.* 2021). We also compared between seasons by solving the model and simulating cohorts of individuals hatching at different times of the year. Finally, we tested the sensitivity of the models by changing the probabilities of dying as function of size and level of infection.

Building the basic model

We used life history data to establish the time horizon and the length of each time step for the model (see Box 1, Fig. 1, Table 1). We modeled the growth of individual frogs using one-week time intervals, starting at hatching, such that the maximum time (T) was 52 weeks (Box 1). The individual frogs in this model were juveniles and early adults classified as young of the year. We modeled discrete size states (S) ranging from 1 to 208, corresponding to different continuous measurable-length unit increases between juveniles and young adults. Size categories were treated as fixed constants, where *Unit 1* represents size upon hatching, *Unit 50* represents size at reproductive maturity, and *Unit 208* represents the maximum size reported for this species. At *Unit 50*, there is a change in growth rate for a given amount of energy to reflect that juveniles and adults grow constantly but at different rates; thus, each size state reflected an increase of 0.44 mm for juveniles and 0.22 mm for adults (Fig. 1a, Box 1, Guarino *et al.* 2019; Joglar 1998; Stewart & Woolbright 1996). Because we were interested in juveniles' growth, we used average mean growth between sexes after maturity. Growth rates tend to decrease in adults because

they reallocate energy for reproduction. The level of infection (I) was modeled logarithmically with eleven states increasing from 0 to 10, with 0 representing an uninfected individual and 1 to 10 corresponding to 10^1 to 10^{10} *Bd* zoospores. This topmost number of zoospores is greater than what is previously reported for the species (Longo *et al.* 2010, 2013), but it can be used as a relative scale for species that are less susceptible or tolerate *Bd*. For simplicity, we only had three values of available energy, the minimum amount needed to include stochasticity while varying the values among seasons and processes. Considering that foraging success is stochastic, we assumed frogs obtained 0, 2, or 4 generic units of useable energy (E) per week, with equal probability, after fulfilling their maintenance energy cost. Individuals must allocate these energy units to one of the three strategies: grow ($i = G$), control infection ($i = C$), or split energy between these two processes ($i = B$) (Fig. 1b). In all cases, size states (S) increased in proportion to the energy allocated to growth depending on the strategy (equation 1),

$$S_{t+1}(i) = \begin{cases} S_t + E, & \text{when } i = G \\ S_t + 0, & \text{when } i = C \\ S_t + \frac{1}{2}E, & \text{when } i = B, \end{cases} \tag{1}$$

where i represents the energy allocation strategy and E represents the generic energy units from foraging. Growth rates increase with temperature (Zuo *et al.* 2012; Álvarez & Nicieza 2002) and food availability (Gomez-Mestre *et al.* 2010). In addition, an increase in temperature at early stages when individuals are still investing energy in development can result in an increase in the developmental rate (e.g., organogenesis and ossification) but not in the growth rate (Gomez-Mestre *et al.* 2010; Orizaola & Laurila 2009). Because both factors can be cofounded in the classification of our seasons and the complexity of development vs. growth at early stages, we only include the energy available in our models. Although reproduction in adults is out of the scope of this model, we can assume that the decrease in growth when reaching the reproductive maturity ($S = 50$) is due to the reallocating of energy from growth to

reproduction (Joglar 1998; Rombough 2006; Taborsky 2006).

Likewise, the level of infection (I) will inherently increase one unit reflecting pathogen exponential growth. It will only decrease in proportion to the amount of energy allocated towards pathogen control (equation 2), and remain as 0 when the individuals do not get infected.

$$I_{t+1}(i) = \begin{cases} I_t + 1 - 0, & \text{when } i = G \\ I_t + 1 - E, & \text{when } i = C \\ I_t + 1 - \frac{1}{2}E, & \text{when } i = B. \end{cases} \tag{2}$$

In the model, we did not assume acquired immunity because the host can clear infections and become re-infected in this system (Box 1). The probability of an uninfected individual becoming infected (P_I) was 0.445, which is the mean *Bd*-prevalence across the year in our study system (Box 1, Fig. S3). An individual can clear an early infection with sustained investment in immunity but only at the expense of growth. We considered that infection levels increased the probability of host death (Longo *et al.* 2013). Thus, in addition to the probability of mortality based on size from causes independent of infection, $M_s(S)$, we also included the infection-based probability of mortality, $M_I(I)$. We modeled size-dependent mortality as a decreasing function of body size based on a log-logistic curve (equation 3, Fig. S1a),

$$M_S(S) = 1 - \left(\frac{M_H}{1 + e^{d(S - S_T)}} \right), \tag{3}$$

where M_H describes the probability of dying in the time horizon, which in our model $M_H = 0.80$ in one year (but see testing sensitivity of the models below). This means that an individual with the smallest size state has a 20% chance of survival in one year. The survival probability in one year is conservative with respect to what has been reported for adults in the species, approximately 94%, considering that juveniles' survival is lower than adults (Stewart 1995). The probability of dying on each time step decreases as size increases at a constant rate according to equation 3 where $d = 0.05$ is the midpoint, and where S_T is the size with the

median probability of dying, $S_T = 50$ in this case. An infected individual probability of dying due to infection level ($M_I(I)$) starts very low at 9×10^{-9}, and logarithmically increases every two levels of infection such as equation 4 (Fig. S1b),

$$M_I(I) = \begin{cases} 0, & \text{for } I = \{0\} \\ 9 \times 10^{-9}, & \text{for } I = \{1,2\} \\ 9 \times 10^{-7}, & \text{for } I = \{3,4\} \\ 9 \times 10^{-5}, & \text{for } I = \{5,6\} \\ 9 \times 10^{-3}, & \text{for } I = \{7,8\} \\ 9 \times 10^{-1}, & \text{for } I = \{9,10\}. \end{cases} \tag{4}$$

The exponential increase in mortality can be associated to the damage cased by the reproduction of the pathogen. We assumed the expected future fitness is a function of final size (*i.e.*, size at time T) and current infection such that equation 5,

$$F(S, I, T) = (1 - M_I(I)) \frac{1}{1 + e^{-0.5(S-100)}}. \tag{5}$$

The future fitness incorporates the expected benefits of being larger (S; Fig. S2) and the probability of surviving expected due to infection ($1 - M_I(I)$). The optimal state-specific strategy ($i \in \{G, C, B\}$) is the one that increases expected future fitness (F), thus we calculated the fitness associated to each investment strategy (v_i) and selected the maximum value (equation 6),

$$F(S, I, t, T) = \max(v_i)\,; \text{where } i \in \{G, C, B\}. \tag{6}$$

The optimal strategy reflects how the state variables size and infection, may change from one time step to another based on the amount of energy frogs find and the energy they allocate to growth and/or control the infection. Calculating v_i takes into account the probability of survival as a function of size ($1 - M_S$) and infection ($1 - M_I$), the probability of finding different amounts of allocatable energy units (pE), the future fitness $F(S, I, t+1, T)$, and the probability of getting infected if uninfected (P_I). Therefore, equation 6 was expanded as detailed in

equations 7 and 8 for infected and uninfected individuals, respectively.

Uninfected individuals are constrained to allocate all available energy to grow, and they can become infected during that time step. Thus, $v_{i=G}$ for these uninfected individuals is as in equation 7. We solved the equation to demonstrate how size and infection change in a one-time step, as detailed below,

$$v_{i=G}(S, I=0, t, T) = 1 - M_{S(t)} \times \left(\begin{array}{c} P_{I(t)} \times \left(\begin{array}{c} \big(p(E|E=0) \times F[S=S_t+0, I=1, t+1]\big) + \\ \big(p(E|E=2) \times F[S=S_t+2, I=1, t+1]\big) + \\ \big(p(E|E=4) \times F[S=S_t+4, I=1, t+1]\big) \end{array} \right) + \\ 1 - P_{I(t)} \times \left(\begin{array}{c} p(E|E=0) \times F[S=S_t+0, I=0, t+1] + \\ p(E|E=2) \times F[S=S_t+2, I=0, t+1] + \\ p(E|E=4) \times F[S=S_t+4, I=0, t+1] \end{array} \right) \end{array} \right) \quad (7)$$

The first term corresponds to the case in which an individual becomes infected and refers to the individuals that survive $(1 - M_S)$ and get infected during the current time step (P_I); future fitness (F) depends on the amount of allocatable energy (E). As a result, the future fitness $(F[S_{t+1,I}, I_{t+1,I}, t+1])$ sets the value of the state variables (S, I, t) on the next time iteration. The second term refers to those individuals that do not get infected during the current time step, indicated by the probability of not getting infected $(1 - P_I)$; as a result, the level of infection remains zero.

In contrast, infected frogs will choose the strategy that maximizes the future fitness (F) among the three energy allocation strategies; thus, equation 6 expands, and changes in state variables are reflected accordingly in equation 8,

$$v_i(S, I>0, t, T, i) = (1 - M_{S(t)}) \times (1 - M_{I(t)}) \times \left(\begin{array}{c} p(E|E=0) \times \\ F[S_{t+1,i}, I_{t+1,i}, t+1] + \\ p(E|E=2) \times \\ F[S_{t+1,i}, I_{t+1,i}, t+1] + \\ p(E|E=4) \times \\ F[S_{t+1,i}, I_{t+1,i}, t+1] \end{array} \right) \forall i \in \{G, C, B\}. \quad (8)$$

In this equation, the probability of getting infected (P_I) is one because individuals are already

infected, thus, it only has one term. However, it considers two mortality probabilities, the probability of surviving due to external causes ($1 - M_S$) and the infection ($1 - M_I$). Because infected individuals can choose among the three energy allocation strategies, the future fitness ($F[S_{t+1,I}, I_{t+1,I}, t+1]$) will depend on the energy they forage and the chosen strategy. We solved these equations to generate a matrix of state-specific optimal decisions for all possible combinations of the three states: size, infection level, and time (Fig. 2a). Next, using state variable elements of the decision matrix, we simulated a population of 100 individuals using Monte Carlo chains to predict realized differences in growth rates, time to maturity, and survival after the growing season in populations following the optimal strategy set. We chose this population size because it is akin to the field data generated from population genomic estimates (Torres-Sánchez & Longo, 2022, Colón-Piñeiro et. al. in prep).

Extending the basic model to include seasonal effects

Direct-developing frogs, like many other taxa, reproduce year-round (Bignotte-Giró *et al.* 2021; Joglar 1998; Townsend & Stewart 1994), which suggests that they can experience suboptimal conditions at some point during their growing period. To examine the cost of the interaction of growing at suboptimal times and the level of infection, we generated new parameter sets for each season (Table 1), solved the models for the optimal behavior, then simulated and evaluated the effects of starting life at four points during the year.

The four temporal scenarios corresponding to frogs that hatch at different times of the year differ in how the seasons occur on the time horizon. Seasons differ in terms of the probability of becoming infected (P_I) and the probability of gaining energy (E) from foraging bouts corresponding with the seasons; two variables that are affected by the seasonality (Box 1, Table 1). We used the prevalence of infection in each season to parameterize the probability of getting infected (P_I) based on the proportion of infected individuals found each season (Box 1, Fig. S3). The pathogenic fungus *Bd* persists all year-around in many populations(*i.e.*,

endemic), including ours, and the infection dynamics respond to environmental conditions associated with seasonality (Hollanders *et al.* 2022; Longo *et al.* 2010; Retallick *et al.* 2004). Assuming that infection solely depends on the contact among individuals to infect new hosts when we know that *Bd* persists in different substrates (Johnson & Speare 2005; Kolby *et al.* 2015 is not a good approximation (Briggs *et al.* 2005). Therefore, we assumed density-independent pathogen transmission. The number of prey and foraging success vary between seasons (Box 1). Thus, we assigned a higher probability of acquiring more energy during the warm than in the cool seasons but constant throughout each. Changing the probability of finding zero to four energy units between seasons is a simplistic way to represent the difference in the amount of energy individuals can obtain from foraging between seasons, which can be scaled based on the study system without requiring more data processing capacity. Thus, the probability of obtaining 0, 2, or 4 units of energy (E) per week from foraging was 0.45, 0.45, and 0.10, respectively, in the cool season and 0.10, 0.45, and 0.45 in the warm season.

Evaluating fitness and infection dynamics at the population level

To evaluate the role of the interaction between seasonality and infections on individuals' fitness, we compared the results among four seasonal scenarios that represent frogs hatching on November–CCWW, February–CWWC, May–WWCC, and August–WCCW. Specifically, we compared among the seasonal scenarios: 1) the set of optimal strategies, 2) the relationship between growth rate (*i.e.*, differences in size states weeks 13 and one for each period divided by 13) and the mean level of infection between cool and warm seasons, and 3) three variables associated to fitness: time to maturity ($S = 50$), and the size and survival at the end of the simulation ($t = 52$). In addition, individuals' tradeoffs in energy allocation between growth and immunity can affect infection dynamics. Although our objectives do not include parameterizing a SIR model, we followed the number of individuals susceptible (S), infected (I), or removed (R; *i.e.*, died) through time. Individuals who die due to the infection or other causes are recorded as removed and remain removed for the rest of the time horizon. Note we

did not distinguished between infection due to contact between hosts or with the environment, but both transmission routes in our model system are mostly associated with seasons (Hollanders *et al.* 2022; Longo *et al.* 2010; Retallick *et al.* 2004), which is accounted in our seasonality models.

Testing sensitivity of the models

To test the robustness of the results, we ran the seasonal scenarios (CCWW, VWWC, WWCC, and WCCW, where W refers to warm and C to cool seasons) varying the probability of dying as a function of size ($M_S(S)$) and as a function of the level of infection ($M_I(I)$). For the probability of dying as a function of size, we set the probabilities of dying of the smallest size state ($S = 1$) in one year (M_H) on equation 3 to 0.2, 0.4, 0.6, and the original set at 0.8 (Fig. S1a). For the probability of dying because of the infection, we used the same step-wise function as in equation 4, but varying the probability of dying due to the highest infection level as a base, set to 0.1, 0.5, 0.9 (original), and 1.0 (Fig. S1b). We chose these values because they represent a range of all potential values including most likely scenarios in nature. We then combine both probabilities in a total of 16 models. Then, we visually compared the density of the four traits associated with fitness, the number of individuals that reached maturity, time to maturity, and the mean body size of individuals and survival at week 52. Models, simulations, and graphs were built in R (Team 2022), setting the seed number to 854354. Script developed to generate the model solution, forward iterations, and the sensitivity analysis, as well as figures, is available during review in a private link from FigShare, https://figshare.com/s/8be08deca455559725a4, and will be made publicly available after publication.

Results

We found that size and level of infection varied with the selected strategy in the optimization model (Fig. 2). When infection levels were very low, the strategy that maximized fitness for most sizes was to allocate all the energy to growth (Fig. 2, $I = 1$), whereas splitting energy between growing and controlling infections was the best strategy when infection was moderate (Fig. 2, $I = 2$ or 3). In contrast, larger size classes typically defended against the pathogen (Fig. 2, $I = 1:3$). However, independent of size, hosts allocated energy to suppress the infection when the pathogen level reached 10^4 zoospores ($I \geq 4$), except when the frogs were near the end of their growing season (> 48 weeks) (Fig. 2). When seasonality was incorporated (Fig. 2b-d), the best strategies to increase future fitness were to grow or grow/control infection during the warm seasons and mainly control infection during the cool seasons when pathogen levels were between 10^2-10^3 zoospores ($I = 2$ or 3). In summary, individuals invested in growth until the level of infection threatened their survival. Then, they shifted to invest in controlling the infection. Moreover, incorporating seasonality (*i.e.*, energy availability, and probability of getting infected) in our optimization model made the optimal strategies more dynamic and demonstrated that individuals must adjust their energy investment strategies according to seasons.

The sets of strategies maximizing future fitness in different models resulted in shifts in growth rates on the forward simulations. The growth rate curve from the simulation using the optimized strategies from the basic model was linear until they reach maturity at state $S = 50$, when the asymptote is observed (Fig. 3a top). In contrast, the slope's steepness differed between seasons in the seasonally-explicit optimization models (Fig. 3a). In addition, our forward simulations revealed the resisted infection thresholds as individuals always kept levels of infection below 10^5 zoospores (Fig. 3a and S4a). The optimized shifts in energy allocation based on the decision matrices (Fig. 2) resulted in increased growth rates when individuals carried low infections (lighter colors) and decreased with higher ones (darker colors) (Fig. 3a).

As expected, our between-model comparisons of growth rates across the mean level of infection varied between models and seasons within models (Fig. 3b and S4b). In both models, the growth rate decreased with the individuals' mean level of infection. However, whereas the decrease in the basic model is constant (Fig. 3b top), the slope and the intercept varied between seasons (Fig. 3b). For example, models showed differences in the intercept between seasons and more variation in infection intensities during the cool season (blue points on Fig. 3b). Moreover, growth rates were always higher, and mean infection levels were always lower in warm than in cool seasons, accurately reflecting the results from the decision matrices (Fig. 2b-d).

Overall, our results showed that the seasons in which frogs hatched significantly influenced their growth and infection trajectories. The best time to hatch for *E. coqui* is at the beginning of the warm season (W-W-C-C) followed by the end of the cool (C-W-W-C; Fig. 4). Although frogs can achieve similar sizes in one year (Fig. 4c), more individuals reached maturity (Fig. 4a) and at a higher rate (Fig. 4b), thus, increasing their likelihood of survival given the seasonal pattern (Fig. 4d). In contrast, the worst scenarios occurred when frogs hatched at the beginning of the cool (C-C-W-W) or at the end of the warm seasons (W-C-C-W) because fewer individuals reached maturity within one year (Fig. 4a), time to maturity was longer to those that arrived (Fig. 4a), and the likelihood of surviving the 52 weeks was lower (Fig. 4c). When testing the sensitivity of the model, we found subtle differences associated with the probability of dying due to the infection level (M_I) but not as a function of size (M_S) (Fig. S5 and Fig. S6). When the probability of dying due to the infection was the highest ($M_I(I = 10) = 1.0$; models with D10 in their y axis labels in Fig. S5 and Fig. S6), the number of individuals reaching maturity (Fig. S5a) and survival at week 52 (Fig. S6b) decreased, while the size at week 52 increased (Fig. S6a). Despite these differences, the best and worst scenarios were the same across models.

The population infection dynamics varied by models and scenarios (5a). In general, the number of susceptible individuals (*i.e.*, non-infected; green in Fig. 5a) decreased at the

beginning and remained close to zero, suggesting that most individuals remained infected with low pathogen burden. When comparing among seasonal scenarios, the number of susceptible individuals is always zero after weeks 11 or 5 in the worst scenarios (CCWW and WCCW, Fig. 5a), meaning that individuals who hatched at the beginning of the cool or middle of the warm seasons can control, but never clear, the infection. Meanwhile, infected individuals (pink in Fig. 5a) hatching at the beginning of the warm (WWCC) or middle of the cool (CWWC) seasons can clear infections and remain uninfected during cool seasons (open circles in Fig. 5a) because the probability of getting infected is lower. As a result, the number of susceptible individuals increased in the cool seasons. In contrast, the mean level of infection in the population is higher during the cool season (open circles in Fig. 5b) than during the warm seasons (filled circles in Fig. 5b). Smaller and/or highly infected individuals had a higher probability of dying (*i.e.*, dead; blue in Fig. 5). The numbers of dying individuals are higher than infected individuals only in the worst scenarios (CCWW and WCCW)(Fig. 5), confirming that the mortality is higher when individuals hatched at the beginning of the cool or at the end of the warm seasons.

Discussion

Hosts across different taxa exhibit variations in their physiological and immunological responses to outbreaks of emerging pathogens (Genersch & Aubert 2010; Kohl *et al.* 2016; Longo *et al.* 2023; Soler *et al.* 2003; Wilder *et al.* 2011). Although mathematical models have been previously used to understand host-pathogen interactions at the population level, our dynamic state variable approach explicitly showed the optimal strategies to increase fitness and how these strategies affect host population dynamics. Overall, our models show that: 1) high levels of infection trigger a reallocation of energy from growth to immune defense; 2) differences in energy availability between seasons exacerbate the effects of this tradeoff; 3) this tradeoff leads to delayed maturity and reduced survival for individuals experiencing a cool

season immediately after hatching; and 4) these tradeoffs influence both population size and host-pathogen dynamics, even when density-dependent interactions are not considered.

Identifying tradeoffs using dynamic optimization models

Our results suggest that an optimal strategy is for individuals to resist or tolerate infection as long as possible, investing in growth and turning to strong defenses when infection levels are high, close to the lethal threshold (Fig. 2). In nature, this pattern is expected because the cost of the immune response is higher than maintenance costs (Derting & Compton 2003). Individuals increase the probability of survival by allocating energy to control and/or clear the infections, but this shift comes at the cost of growth, resulting in delayed maturity (Fig. 3). Surprisingly, we did not observe significant size differences between simulations. However, individuals with higher mean infection levels were smaller within each simulation. These results indicate that energy allocation to control the infection produces smaller individuals (Burrowes *et al.* 2008). In other systems, individuals exhibit elevated wound healing capacity at the cost of lower growth rates (Korfel *et al.* 2015) and delayed maturity (Saumier *et al.* 1986). Because body size and time to maturity are associated with fitness and recruitment (Hilderbrand *et al.* 2019; Scheele *et al.* 2024; Townsend & Stewart 1994; Wise & Jaeger 2021), future fitness should be accounted for when evaluating population viability after disease outbreaks.

Our models emphasized the tradeoff between energy allocated to control the infection versus growth, and our results align with natural observations (Burrowes *et al.* 2008). However, we recognize that a mosaic of interacting mechanisms can result in size differences between infected and non-infected individuals. For example, frogs might experience a downward spiral where infection prevents them from acquiring adequate energy due to reduced appetite or foraging success during disease (Carter *et al.* 2020; Peterson *et al.* 2013; Venesky *et al.* 2009). Additionally, immune diversity may increase with age, with larger individuals carrying more

receptors related to acquired resistance (Savage & Zamudio 2011). Thus, we propose experiments manipulating food intake followed by pathogen exposure to confirm the mechanisms responsible for these growth-defense tradeoffs.

Seasonality exacerbates the growth-defense tradeoffs

Host-pathogen dynamics and food availability vary by season (Longo *et al.* 2010; Stewart & Woolbright 1996). We expected the season in which individuals hatch would exacerbate differences in the growth-defense tradeoff in energy allocation and growth rate. When analyzed at the population level (*i.e.*, 100 individuals simulated per scenario), frogs body size at one year did not vary across models because they mostly chose to invest in growth, which is critical at early stages to increase survival (Altwegg & Reyer 2003; Taborsky 2006). To compensate for size, individuals use two mechanisms: increasing growth rate after a period of poor nutrition and reduced growth, as shown by the spline pattern driven by higher growth rates during warm seasons in Fig. 3a; or by delaying maturity, as in Fig. 4a (Finkielstain *et al.* 2013; Metcalfe & Monaghan 2001). In nature, compensation can be even higher because the growth rates increase with warmer temperatures (Colón-Piñeiro 2017). However, compensatory growth after poor nutrition provides short-term advantages but comes at a cost, ranging from reduced locomotion performance to a shorter lifespan (reviewed in Metcalfe & Monaghan 2001).

The growth-defense tradeoff results in higher pathogen loads, particularly under low food availability (Guyer 1988; Schiesari *et al.* 2006). Consistent with previous studies in natural frog populations (Garnham *et al.* 2022; Longo *et al.* 2010), higher levels of infections near and above 10^4 *Bd* zoospores ($I > 4$) were only observed during the cool season when seasonality was included. Although the prevalence (number of infected individuals) was lower in the cool seasons, the mean pathogen burden of the population was higher, indicating that infected individuals carried more *Bd* zoospores. In the tropics, drier seasons are associated with cooler

temperatures (Longo *et al.* 2010), and drought-related stress makes frogs more susceptible to pathogens (Longo *et al.* 2010) while *Bd* operates optimally at lower temperatures (Van Rooij *et al.* 2015). Additionally, the density of individuals in nature varies among seasons (Stewart 1995, Colón-Piñeiro et al., in review) and can affect host-pathogen interactions due to higher shedding rates (Garnham *et al.* 2022) or physical contact among individuals (Adams *et al.* 2017; Kupferberg *et al.* 2022) in cool-dry seasons. Our simulations showed differences in the density of individuals, even without considering density dependence in host transmission. Thus, longer, cooler, and drier seasons will be devastating for amphibians already threatened by emergent pathogens and climate change in the tropics and worldwide (Guirguis *et al.* 2023; Scheele *et al.* 2019).

Poor parental decisions influenced future fitness traits

Our model also predicts that seasonality affects time to maturity and survival (Fig. 3a, S2, and 4a,c), which can have carryover effects on long-term population viability (Cabrera-Guzmán *et al.* 2013). Hatching at the end of the warm season was unfavorable, likely due to increased disease mortality risks, smaller size, and high infection rates. Because parents determine the hatching season, our models indicate that reproducing during the cool season results in lower offspring fitness. We speculate that reproduction at suboptimal times may occur when high-fitness individuals reproduce a second time in a year or low-fitness individuals that failed to mate during the warm season (Höbel *et al.* 2021; Townsend & Stewart 1994). Regardless of parental fitness, reproduction during the cool (and usually dry) season decreases the survival probability of the offspring due to additional stressors, including reduced water availability, weaker immune responses, and exposure to less diverse microbiomes (Le Sage *et al.* 2021; Longo *et al.* 2015). Future empirical research with longitudinal data could validate our model predictions on recruitment and survival.

Potential applications of dynamic models in conservation

Understanding these interactions is particularly important for predicting population recruitment amid extreme climatic events (Planton *et al.* 2008; Ummenhofer & Meehl 2017). For example, prolonged droughts can disrupt animal communities, including frogs and their prey (Lister & Garcia 2018). Climate models anticipate longer and more irregular dry seasons (Neelin *et al.* 2006; Nurse & Sem 2001; Team *et al.* 2015), challenging amphibian adaptability. Our study focuses on tropical ecosystems with warm-wet and cool-dry seasons (Burrowes *et al.* 2004), but by adjusting parameter values, our dynamic model can predict outcomes in other bioclimatic zones under different climate scenarios, including disease outbreaks and extreme droughts. While we focused on pathogens, future models could include parasitic energy drains (Graham 2008; Ramesh & Hall 2023) by adjusting energy losses during infections. Shifts in season duration and increases in extreme weather events pose extinction risks (Parmesan *et al.* 2000), especially for species recovering from initial pathogen outbreaks.

Conservation programs breed threatened species for reintroduction, for example, amphibian species threatened by *Bd* (Harding *et al.* 2016). These initiatives require population viability analysis and modeling to assess disease impacts on reintroduction success (Ballou 1993). Extensions of our model may allow researchers to predict the best time to release individuals into the wild based on reproductive patterns and infection risk. The response to infections and seasons depends on the intrinsic traits of the host and the pathogen and is context-specific (Civitello *et al.* 2018). Because the state variables are relative to the system, our model can be extended to other scenarios and endangered taxa, providing key conservation insights. We hope conservation efforts include dynamic modeling to increase reintroduction success.

Conclusions and future directions

Our results demonstrate that flexible energy allocation strategies promote survival and fitness under different pathogen pressures. Individuals are expected to prioritize growth over

infection control, tolerating infections rather than sacrificing growth unnecessarily. Frogs only allocated energy to control infections at sub-lethal levels, leading to delayed maturation and potential long-term fitness impacts (Hilderbrand *et al.* 2019; Townsend & Stewart 1994; Wise & Jaeger 2021) (Scheele *et al.* 2024). Our models also demonstrated that individuals can slightly compensate for a "bad start" due to seasonality by growing faster during transitions or delaying maturity (Finkielstain *et al.* 2013; Metcalfe & Monaghan 2001; Székely *et al.* 2020). Finally, our models revealed that the energy allocation tradeoffs to increase future fitness affect population size and infection without density dependence on host-pathogen interactions. Common-garden experiments can provide empirical evidence for these predictions. For example, experiments varying food availability according to seasonal patterns could reveal more about the consequences of infection across life-history stages. In addition, modeling the reproduction-defense tradeoffs in adults can be coupled with our model to increase our understanding of how pathogens drive population dynamics under different climatic scenarios. Our research highlights the utility of dynamic state variable models, which can be extended to multiple species and conditions (*e.g.*, extreme droughts, pathogen outbreaks, and species reintroduction for conservation) by adjusting parameter values with empirical data collected from experiments or field observations.

Acknowledgments

We thank O. Acevedo-Charry, our colleagues from the Dynamic Optimization Models course, PEERs, and the Longo Lab at UF-Biology, as well as the reviewers, for their input and thoughtful discussions about earlier versions of the models presented in this paper. Funding was provided by the National Science Foundation (NSF-IOS-2011281, 2011278, NSFDDIG-1310036), the Hispanic Scholarship Fund, The Society for Integrative and Comparative Biology, the Department of Biology, the Biodiversity Institute at the University of Florida, American Society of Naturalists, and the American Association for University Women

(AAUW 7223748). St. Mary's participation in this project was partially supported by the NSF IR/D program.

Author Contributions

Conceptualization: ZCP, AVL; model development: ZCP, NWM, CStM, TJK, and BLB; coding and data visualization: NWM, ZCP; data analysis: ZCP, CStM, AVL, PAB, and MAA; funding acquisition: AVL, PAB; writing the first draft of the manuscript: ZCP, AVL. All co-authors contributed substantially to the revisions and editing of the manuscript and approved the final version.

Conflict of Interest statement

The authors declare no conflicts of interest.

Data availability statement

Script developed to generate backward, forward iterations, and the sensitivity analysis, as well as figures, is available during review a private link from FigShare, https://figshare.com/s/8be08deca455559725a4, and will be available after publication.

ORCID

Zuania Colón-Piñeiro: https://orcid.org/0000-0003-0508-2538

Nich W. Martin: https://orcid.org/0000-0001-9539-250X

Travis J Klee: https://orcid.org/0009-0000-9545-7801

Colette M St. Mary: https://orcid.org/0000-0002-3175-5284

Miguel Acevedo: https://orcid.org/0000-0002-8289-1497

Patricia Burrowes: https://orcid.org/0000-0002-3085-6681

Ana V. Longo: https://orcid.org/0000-0002-5112-1246

References

Adams, A. J., Kupferberg, S. J., Wilber, M. Q., Pessier, A. P., Grefsrud, M., Bobzien, S., Vredenburg, V. T. & Briggs, C. J. (2017). Extreme drought, host density, sex, and bullfrogs influence fungal pathogen infection in a declining lotic amphibian. *Ecosphere*, 8, e01740.

Alizon, S., Hurford, A., Mideo, N. & Van Baalen, M. (2009). Virulence evolution and the trade-off hypothesis: history, current state of affairs and the future: Virulence evolution and trade-off hypothesis. *Journal of Evolutionary Biology*, 22, 245–259.

Altizer, S., Dobson, A., Hosseini, P., Hudson, P., Pascual, M. & Rohani, P. (2006). Seasonality and the dynamics of infectious diseases. *Ecology Letters*, 9, 467–484.

Altwegg, R. & Reyer, H.-U. (2003). Patterns of natural selection on size at metamorphosis in water frogs. *Evolution*, 57, 872–882.

Alvarado-Rybak, M. & Azat, C. (2021). Chytridiomycosis outbreak in a Chilean giant frog (*Calyptocephalella gayi*) captive breeding program: Genomic characterization and pathological findings. *Frontiers in Veterinary Science*, 8, 9.

Andreasen, V. & Dwyer, G. (2023). Seasonality and the coexistence of pathogen strains. *The American Naturalist*, 201, 639–658.

Ballou, J. D. (1993). Assessing the risks of infectious diseases in captive breeding and reintroduction programs. *Journal of Zoo and Wildlife Medicine*, 327–335.

Berger, L., Speare, R. & Skerratt, L. (2005). Distribution of *Batrachochytrium dendrobatidis* and pathology in the skin of green tree frogs *Litoria caerulea* with severe chytridiomycosis. *Diseases of Aquatic Organisms*, 68, 65–70.

Bignotte-Giró, I., López-Iborra, G. M., Ramírez-Pinilla, M. P. & Fong G., A. (2021). Reproductive phenology of five species of terrestrial frogs (Genus *Eleutherodactylus*) from Cuba. *Journal of Herpetology*, 55, 127–136.

Brannelly, L. A., McCallum, H. I., Grogan, L. F., Briggs, C. J., Ribas, M. P., Hollanders, M., Sasso, T., Familiar López, M., Newell, D. A. & Kilpatrick, A. M. (2021a). Mechanisms underlying host persistence following amphibian disease emergence determine appropriate management strategies. *Ecology Letters*, 24, 130–148.

Brannelly, L. A., Webb, R. J., Jiang, Z., Berger, L., Skerratt, L. F. & Grogan, L. F. (2021b). Declining amphibians might be evolving increased reproductive effort in the face of devastating disease. *Evolution*, 75, 2555–2567.

Breckling, B. (2002). Individual-based modelling potentials and limitations. *The Scientific World Journal*, 2, 1044–1062.

Briggs, C. J., Vredenburg, V. T., Knapp, R. A. & Rachowicz, L. J. (2005). Investigating the population-level effects of chytridiomycosis: an emerging infectious disease of amphibians. *Ecology*, 86, 3149–3159.

Burrowes, P. A., Joglar, R. L. & Green, D. E. (2004). Potential causes for amphibian declines in puerto rico. *Herpetologica*, 60, 141–154.

Burrowes, P. A., Longo, A. V. & Rodríguez, C. A. (2008). Potential fitness cost of *Batrachochytrium dendrobatidis* in *Eleutherodactylus coqui*, and comments on environment-related risk of infection. *Herpetotropicos*, 4, 51–57.

Cabrera-Guzmán, E., Crossland, M. R., Brown, G. P. & Shine, R. (2013). Larger body size at metamorphosis Enhances Survival, growth and Performance of young cane toads (*Rhinella marina*). *PLoS ONE*, 8, e70121.

Carter, E. D., Miller, D. L., Peterson, A. C., Sutton, W. B., Cusaac, J. P. W., Spatz, J. A., Rollins-Smith, L., Reinert, L., Bohanon, M., Williams, L. A. *et al.* (2020). Conservation risk of batrachochytrium salamandrivorans to endemic lungless salamanders. *Conservation Letters*, 13, e12675.

Civitello, D. J., Allman, B. E., Morozumi, C. & Rohr, J. R. (2018). Assessing the direct and indirect effects of food provisioning and nutrient enrichment on wildlife infectious disease dynamics. *Philosophical Transactions of the Royal Society B: Biological Sciences*, 373, 20170101.

Clark, C. W. & Mangel, M. (2000). *Dynamic state variable models in ecology: methods and applications*. Oxford University Press.

Colón-Piñeiro, Z. (2017). *Efecto de la temperatura sobre el desarrollo de Eleutherodactylus coqui: integración entre mecanismos que influencian el fenotipo*. Ph.D. thesis, Universidad de Puerto Rico, San Juan, Puerto Rico.

Cressler, C. E., Nelson, W. A., Day, T. & McCauley, E. (2014). Disentangling the interaction among host resources, the immune system and pathogens. *Ecology letters*, 17, 284–293.

Derting, T. & Compton, S. (2003). Immune response, not immune maintenance, is energetically costly in wild white-footed mice (*Peromyscus leucopus*). *Physiological and Biochemical Zoology*, 76, 744–752.

DiRenzo, G. V., Che-Castaldo, C., Saunders, S. P., Campbell Grant, E. H. & Zipkin, E. F. (2019). Disease-structured N -mixture models: A practical guide to model disease dynamics using count data. *Ecology and Evolution*, 9, 899–909.

Drewry, G. E. (1970). The role of amphibians in the ecology of Puerto Rican rain forest. In: *The rain forest project annual report*. Puerto Rico Nuclear Center, AEC-UPR, Puerto Rico, pp. 16–63.

Dushoff, J. (1999). Host heterogeneity and disease endemicity: A moment-based approach. *Theoretical Population Biology*, 56, 325–335.

Dwyer, G., Elkinton, J. & Buonaccorsi, J. (1997). Host heterogeneity in susceptibility and disease dynamics: Tests of a mathematical model. *The American Naturalist*, 150, 685–707.

El-Sayed, A. & Kamel, M. (2020). Climatic changes and their role in emergence and re-emergence of diseases. *Environmental Science and Pollution Research*, 27, 22336–22352.

Finkielstain, G., Lui, J. & Baron, J. (2013). Catch-up growth: cellular and molecular mechanisms. *Nutrition and Growth*, 106, 100–104.

Fleming-Davies, A. E., Dukic, V., Andreasen, V. & Dwyer, G. (2015). Effects of host heterogeneity on pathogen diversity and evolution. *Ecology letters*, 18, 1252–1261.

French, S. S., DeNardo, D. F. & Moore, M. C. (2007). Trade-offs between the reproductive and immune systems: facultative responses to resources or obligate responses to reproduction? *The American Naturalist*, 170, 79–89.

Garner, T. W. J., Walker, S., Bosch, J., Leech, S., Marcus Rowcliffe, J., Cunningham, A. A. & Fisher, M. C. (2009). Life history tradeoffs influence mortality associated with the amphibian pathogen *Batrachochytrium dendrobatidis*. *Oikos*, 118, 783–791.

Garnham, J., Bower, D., Stockwell, M., Pickett, E., Pollard, C., Clulow, J. & Mahony, M. (2022). Seasonal variation in the prevalence of a fungal pathogen and unexpected clearance from infection in a susceptible frog species. *Diseases of Aquatic Organisms*, 148, 1–11.

Garrison, R. W. & Willig, M. R. (1996). Arboreal invertebrates. In: *The food web of a tropical rain forest*. The University of Chicago Press, Chicago and London, pp. 183–246.

Genersch, E. & Aubert, M. (2010). Emerging and re-emerging viruses of the honey bee (*Apis mellifera* L.). *Veterinary Research*, 41, 54.

Gomez-Mestre, I., Saccoccio, V. L., Iijima, T., Collins, E. M., Rosenthal, G. G. & Warkentin, K. M. (2010). The shape of things to come: linking developmental plasticity to post-metamorphic morphology in anurans: developmental plasticity in frogs. *Journal of Evolutionary Biology*, 23, 1364–1373.

Graham, A. L. (2008). Ecological rules governing helminth–microparasite coinfection. *Proceedings of the National Academy of Sciences*, 105, 566–570.

Graham, M., Ayabina, D., Lucas, T. C., Collyer, B. S., Medley, G. F., Hollingsworth, T. D. & Toor, J. (2021). SCHISTOX: An individual based model for the epidemiology and control of schistosomiasis. *Infectious Disease Modelling*, 6, 438–447.

Grogan, L. F., Humphries, J. E., Robert, J., Lanctôt, C. M., Nock, C. J., Newell, D. A. & McCallum, H. I. (2020). Immunological aspects of chytridiomycosis. *Journal of Fungi*, 6, 234.

Guarino, F. M., Crottini, A., Mezzasalma, M., Randrianirina, J. E. & Andreone, F. (2019). A skeletochronological estimate of age and growth in a large riparian frog from Madagascar (Anura, Mantellidae, *Mantidactylus*). *Herpetozoa*, 32, 39–44.

Guirguis, J., Goodyear, L. E., Finn, C., Johnson, J. V. & Pincheira-Donoso, D. (2023). Risk of extinction increases towards higher elevations across the world's amphibians. *Global Ecology and Biogeography*, 32, 1952–1963.

Guyer, C. (1988). Food supplementation in a tropical mainland anole, *Norops humilis*: effects on individuals. *Ecology*, 69, 362–369.

Hall, J. M., Mitchell, T. S., Thawley, C. J., Stroud, J. T. & Warner, D. A. (2020). Adaptive seasonal shift towards investment in fewer, larger offspring: Evidence from field and laboratory studies. *Journal of Animal Ecology*, 89, 1242–1253.

Harding, G., Griffiths, R. A. & Pavajeau, L. (2016). Developments in amphibian captive breeding and reintroduction programs. *Conservation Biology*, 30, 340–349.

Hilderbrand, G. V., Gustine, D. D., Joly, K., Mangipane, B., Leacock, W., Cameron, M. D., Sorum, M. S., Mangipane, L. S. & Erlenbach, J. A. (2019). Influence of maternal body size, condition, and age on recruitment of four brown bear populations. *Ursus*, 29, 111.

Hollanders, M., Grogan, L. F., Nock, C. J., McCallum, H. I. & Newell, D. A. (2022). Recovered frog populations coexist with endemic *Batrachochytrium dendrobatidis* despite load-dependent mortality. *Ecological Applications*.

Huot, B., Yeo, J., Montgomery, B. L. & He, S. Y. (2014). Growth–defense tradeoffs in plants: A balancing act to optimize fitness. *Molecular Plant*, 7, 1267–1287.

Höbel, G., Kolodziej, R., Nelson, D. & White, C. (2021). Effect of body size, age and timing of breeding on clutch and egg size of female eastern gray treefrogs, *Hyla versicolor*. *Amphibia-Reptilia*, 43, 25–35.

Joglar, R. J. (1998). *Los coquies de Puerto Rico: su historia natural y conservación*. 1st edn. Editorial de la Universidad de Puerto Rico, San Juan.

Johnson, M. & Speare, R. (2005). Possible modes of dissemination of the amphibian chytrid *Batrachochytrium dendrobatidis* in the environment. *Diseases of Aquatic Organisms*, 65, 181–186.

Keehnen, N. L. P., Kučerová, L., Nylin, S., Theopold, U. & Wheat, C. W. (2021). Physiological tradeoffs of immune response differs by infection type in *Pieris napi*. *Frontiers in Physiology*, 11, Article 576797.

Kohl, W. T., McClure, T. I. & Miner, B. G. (2016). Decreased temperature facilitates short-term sea star wasting disease survival in the keystone intertidal sea star *Pisaster ochraceus*. *PLOS ONE*, 11, e0153670.

Kolby, J. E., Ramirez, S. D., Berger, L., Richards-Hrdlicka, K. L., Jocque, M. & Skerratt, L. F.

(2015). Terrestrial dispersal and potential environmental transmission of the amphibian chytrid Fungus (*Batrachochytrium dendrobatidis*). *PLOS ONE*, 10, e0125386.

Korfel, C. A., Chamberlain, J. D. & Gifford, M. E. (2015). A test of energetic trade-offs between growth and immune function in watersnakes. *Oecologia*, 179, 343–351.

Kupferberg, S. J., Moidu, H., Adams, A. J., Catenazzi, A., Grefsrud, M., Bobzien, S., Leidy, R. & Carlson, S. M. (2022). Seasonal drought and its effects on frog population dynamics and amphibian disease in intermittent streams. *Ecohydrology*, 15, e2395.

Langhammer, P. F., Burrowes, P. A., Lips, K. R., Bryant, A. B. & Collins, J. P. (2014). Susceptibility to the amphibian chytrid fungus varies with ontogeny in the direct-developing frog, *Eleutherodactylus coqui*. *Journal of Wildlife Diseases*, 50, 438–446.

Le Sage, E. H., LaBumbard, B. C., Reinert, L. K., Miller, B. T., Richards-Zawacki, C. L., Woodhams, D. C. & Rollins-Smith, L. A. (2021). Preparatory immunity: Seasonality of mucosal skin defences and *Batrachochytrium* infections in southern leopard frogs. *Journal of Animal Ecology*, 90, 542–554.

Lister, B. C. & Garcia, A. (2018). Climate-driven declines in arthropod abundance restructure a rainforest food web. *PNAS*, 115, E10397–E10406.

Longo, A. V., Burrowes, P. & Joglar, R. (2010). Seasonality of *Batrachochytrium dendrobatidis* infection in direct-developing frogs suggests a mechanism for persistence. *Diseases of Aquatic Organisms*, 92, 253–260.

Longo, A. V. & Burrowes, P. A. (2010). Persistence with chytridiomycosis does not assure survival of direct-developing frogs. *EcoHealth*, 7, 185–195.

Longo, A. V., Lips, K. R. & Zamudio, K. R. (2023). Evolutionary ecology of host competence after a chytrid outbreak in a naive amphibian community. *Philosophical Transactions of the Royal Society B*, 378, 20220130.

Longo, A. V., Ossiboff, R. J., Zamudio, K. R. & Burrowes, P. A. (2013). Lability in host defenses: terrestrial frogs die from chytridiomycosis under enzootic conditions. *Journal of Wildlife Diseases*, 49, 197–199.

Longo, A. V., Savage, A. E., Hewson, I. & Zamudio, K. R. (2015). Seasonal and ontogenetic variation of skin microbial communities and relationships to natural disease dynamics in declining amphibians. *Royal Society Open Science*, 2, 140377.

Mangel, M. & Clark, C. W. (1988). *Dynamic modeling in behavioral ecology*. Princeton University Press, New Jersey, USA.

McCauley, S. J., Bouchard, S. S., Farina, B. J., Isvaran, K., Quader, S., Wood, D. W. & St. Mary, C. M. (2000). Energetic dynamics and anuran breeding phenology: insights from a dynamic game. *Behavioral Ecology*, 11, 429–436.

McNamara, J. M. & Houston, A. I. (1986). The common currency for behavioral decisions. *The American Naturalist*, 127, 358–378.

Metcalfe, N. B. & Monaghan, P. (2001). Compensation for a bad start: grow now, pay later? *Trends in Ecology & Evolution*, 16, 254–260.

Miller, M., White, A. & Boots, M. (2005). The evolution of host resistance: Tolerance and control as distinct strategies. *Journal of Theoretical Biology*, 236, 198–207.

Neelin, J. D., Münnich, M., Su, H., Meyerson, J. E. & Holloway, C. E. (2006). Tropical drying trends in global warming models and observations. *Proceedings of the National Academy of Sciences*, 103, 6110–6115.

Nelson, R. J. (2004). Seasonal immune function and sickness responses. *Trends in Immunology*, 25, 187–192.

Nurse, L. & Sem (2001). Small islands states. In: *Climate Change 2001: Impacts, Adaptation &*

Vulnerability (eds. McCarthy, J., Canziani, O., Leary, N., Dokken, D. & White, K.). Cambridge University Press, pp. 842–875.

Orizaola, G. & Laurila, A. (2009). Microgeographic variation in temperature-induced plasticity in an isolated amphibian metapopulation. *Evolutionary Ecology*, 23, 979–991.

Parmesan, C., Root, T. L. & Willig, M. R. (2000). Impacts of extreme weather and climate on terrestrial biota. *Bulletin of the American Meteorological Society*, 81, 443–450.

Peterson, J. D., Steffen, J. E., Reinert, L. K., Cobine, P. A., Appel, A., Rollins-Smith, L. & Mendonça, M. T. (2013). Host stress response is important for the pathogenesis of the deadly amphibian disease, chytridiomycosis, in *Litoria caerulea*. *PLoS ONE*, 8, e62146.

Planton, S., Déqué, M., Chauvin, F. & Terray, L. (2008). Expected impacts of climate change on extreme climate events. *Philosophical Transactions of the Royal Society B: Biological Sciences*, 340, 564–574.

Pough, F. H., Taigen, T. L., Stewart, M. M. & Brussard, P. F. (1983). Behavioral modification of evaporative water loss by a Puerto Rican frog. *Ecology*, 64, 244–252.

Ramesh, A. & Hall, S. R. (2023). Niche theory for within-host parasite dynamics: Analogies to food web modules via feedback loops. *Ecology Letters*, 26, 351–368.

Retallick, R. W. R., McCallum, H. & Speare, R. (2004). Endemic infection of the amphibian chytrid fungus in a frog community post-decline. *PLoS biology*, 2, e351.

Rombough, P. (2006). Developmental costs and the partitioning of metabolic energy. *Comparative Developmental Physiology: Contributions, Tools and Trends*, 216.

Rumschlag, S. L. & Boone, M. D. (2020). Lethal and sublethal amphibian host responses to *Batrachochytrium dendrobatidis* exposure are determined by the additive influence of host resource availability. *Journal of Wildlife Diseases*, 56, 338–349.

Saumier, M. D., Rau, M. E. & Bird, D. M. (1986). The effect of trichinella pseudospiralis infection on the reproductive success of captive american kestrels (falco sparverius). *Canadian Journal of Zoology*, 64, 2123–2125.

Savage, A. E. & Zamudio, K. R. (2011). MHC genotypes associate with resistance to a frog-killing fungus. *Proceedings of the National Academy of Sciences*, 108, 16705–16710.

Scheele, B., Webb, R., Hua, X. & Hollanders, M. (2024). Variation in amphibian maturation rates influences population vulnerability to disease-induced declines. *Animal Conservation*, acv.12939.

Scheele, B. C., Pasmans, F., Skerratt, L. F., Berger, L., Martel, A., Beukema, W., Acevedo, A. A., Burrowes, P. A., Carvalho, T., Catenazzi, A., De la Riva, I., Fisher, M. C., Flechas, S. V., Foster, C. N., Frías-Álvarez, P., Garner, T. W. J., Gratwicke, B., Guayasamin, J. M., Hirschfeld, M., Kolby, J. E., Kosch, T. A., La Marca, E., Lindenmayer, D. B., Lips, K. R., Longo, A. V., Maneyro, R., McDonald, C. A., Mendelson, J., Palacios-Rodriguez, P., Parra-Olea, G., Richards-Zawacki, C. L., Rödel, M.-O., Rovito, S. M., Soto-Azat, C., Toledo, L. F., Voyles, J., Weldon, C., Whitfield, S. M., Wilkinson, M., Zamudio, K. R. & Canessa, S. (2019). Amphibian fungal panzootic causes catastrophic and ongoing loss of biodiversity. *Science*, 363, 1459–1463.

Schiesari, L., Peacor, S. D. & Werner, E. E. (2006). The growth–mortality tradeoff: evidence from anuran larvae and consequences for species distributions. *Oecologia*, 149, 194–202.

Shudo, E. & Iwasa, Y. (2004). Dynamic optimization of host defense, immune memory, and post-infection pathogen levels in mammals. *Journal of Theoretical Biology*, 228, 17–29.

Simon, M. W., Barfield, M. & Holt, R. D. (2022). When growing pains and sick days collide: infectious disease can stabilize host population oscillations caused by stage structure. *Theoretical Ecology*, 15, 285–309.

Soler, J. J., Neve, L. d., Pérez–Contreras, T., Soler, M. & Sorci, G. (2003). Trade-off between

immunocompetence and growth in magpies: an experimental study. *Proceedings of the Royal Society of London. Series B: Biological Sciences*, 270, 241–248.

Stearns, S. C. (2000). Life history evolution: successes, limitations, and prospects. *Naturwissenschaften*, 87, 476–486.

Stephenson, J. F., Young, K. A., Fox, J., Jokela, J., Cable, J. & Perkins, S. E. (2017). Host heterogeneity affects both parasite transmission to and fitness on subsequent hosts. *Philosophical Transactions of the Royal Society B: Biological Sciences*, 372, 20160093.

Stewart, M. M. (1995). Climate driven population fluctuations in rain forest frogs. *Journal of Herpetology*, 29, 437–446.

Stewart, M. M. & Woolbright, L. L. (1996). Amphibians. In: *The food web of a tropical rain forest*, 1st edn. The University of Chicago Press, Chicago. ISBN 0-226-70600-1, pp. 273–320.

Székely, D., Cogălniceanu, D., Székely, P., Armijos-Ojeda, D., Espinosa-Mogrovejo, V. & Denoël, M. (2020). How to recover from a bad start: size at metamorphosis affects growth and survival in a tropical amphibian. *BMC Ecology*, 20, 24.

Taborsky, B. (2006). The influence of juvenile and adult environments on life-history trajectories. *Proceedings of the Royal Society B: Biological Sciences*, 273, 741–750.

Team, C. W., Pachauri, R. K. & Mayer, L., eds. (2015). *Climate change 2014: synthesis report*. Intergovernmental Panel on Climate Change, Geneva, Switzerland. ISBN 978-92-9169-143-2.

Team, R. C. (2022). R: A language and environment for statistical computing. URL `http://www.R-project.org/`.

Torres-Sánchez, M. & Longo, A. V. (2022). Linking pathogen–microbiome–host interactions to explain amphibian population dynamics. *Molecular Ecology*, 31, 5784–5794.

Townsend, D. S. & Stewart, M. M. (1994). Reproductive ecology of the Puerto Rican frog *Eleutherodactylus coqui*. *Journal of Herpetology*, 28, 34.

Townsend, D. S., Stewart, M. M. & Pough, F. H. (1984). Male parental care and its adaptive significance in a neotropical frog. *Animal Behaviour*, 32, 421–431.

Townsend, D. S., Stewart, M. M., Pough, F. H. & Brussard, P. F. (1981). Internal fertilization in an oviparous frog. *Science*, 212, 469–471.

Ummenhofer, C. C. & Meehl, G. A. (2017). Extreme weather and climate events with ecological relevance: a review. *Philosophical Transactions of the Royal Society B: Biological Sciences*, 372, 1–13.

Van Rooij, P., Martel, A., Haesebrouck, F. & Pasmans, F. (2015). Amphibian chytridiomycosis: a review with focus on fungus-host interactions. *Veterinary Research*, 46, 137.

Venesky, M. D., Parris, M. J. & Storfer, A. (2009). Impacts of *Batrachochytrium dendrobatidis* infection on tadpole foraging performance. *EcoHealth*, 6, 565–575.

Wilder, A. P., Frick, W. F., Langwig, K. E. & Kunz, T. H. (2011). Risk factors associated with mortality from white-nose syndrome among hibernating bat colonies. *Biology Letters*, 7, 950–953.

Wise, S. E. & Jaeger, R. G. (2021). Maternal body size and condition predict measures of reproductive success and future reproductive allocation in territorial eastern red-backed salamanders. *Ichthyology & Herpetology*, 109.

Woolbright, L. L. (1983). Sexual selection and size dimorphism in anuran Amphibia. *The American Naturalist*, 121, 110–119.

Woolbright, L. L. & Stewart, M. M. (1987). Foraging success of the tropical frog, *Eleutherodactylus coqui*: The cost of calling. *Copeia*, 1987, 69–75.

Zuo, W., Moses, M. E., West, G. B., Hou, C. & Brown, J. H. (2012). A general model for effects of temperature on ectotherm ontogenetic growth and development. *Proceedings of the Royal Society B: Biological Sciences*, 279, 1840–1846.

Álvarez, D. & Nicieza, A. G. (2002). Effects of induced variation in anuran larval development on postmetamorphic energy reserves and locomotion. *Oecologia*, 131, 186–195.

Box 1

Natural history: *Eleutherodactylus coqui*, the coqui, is a tropical direct-developing frog endemic to Puerto Rico. Direct-developing frogs evolved to bypass the tadpole stage and emerge from the egg as miniature adults in terrestrial environments. Reproduction occurs throughout the entire year (Bignotte-Giró *et al.* 2021; Joglar 1998; Townsend & Stewart 1994), fertilization is internal (Townsend *et al.* 1981), and male parents take care of the clutch during the entire pre-hatching developmental period and even a few days after hatching (Joglar 1998; Townsend *et al.* 1984). Thus, we expect fitness costs to have their greatest effects during early life-history stages, particularly when newborn frogs hatch at suboptimal times. The likelihood of survival in juveniles is further diminished by environmental stress because individual mortality is expected after prolonged dry periods of five days (Stewart 1995). Coqui frogs hatch at a snout-to-vent length (SVL) of 6 mm on average (Colón-Piñeiro 2017) and take approximately nine months to one year to reach maturity (Joglar 1998; Woolbright 1983) at $\approx$ 28 mm, independent of sex (Stewart & Woolbright 1996; Townsend & Stewart 1994). Like many amphibians, coquis constantly grow until reaching sexual maturity, when growth rates decrease and vary between sexes (Guarino *et al.* 2019; Stewart & Woolbright 1996); the maximum size reported for an adult female is 63 mm (Joglar 1998J). In addition, parental care can increase infection risk of the offspring due to close contact of newborns with sloughing skin from the male.

Despite less drastic temperature changes in the tropics than in temperate zones, the diversity and abundance of amphibians' prey change over time (Garrison & Willig 1996). Likewise, field studies have demonstrated reduced stomach content of tropical frogs during the dry season (Pough *et al.* 1983; Stewart & Woolbright 1996; Woolbright & Stewart 1987). Collectively, these findings suggest seasonal differences in resource availability for coqui frogs.

Host-pathogen dynamics: In our previous studies, we have primarily shown pathogen infection affecting adult mortality, but identified infected juveniles as a vulnerable life-history

stage (Langhammer *et al.* 2014; Longo & Burrowes 2010; Longo *et al.* 2015). Coqui frogs can become reinfected after clearing the pathogen, suggesting no acquired immunity (unpublished data, Longo & Burrowes). The coqui-*Bd* interactions vary between seasons, where the prevalence of infection is higher during the warm periods (unpublished data, Longo & Burrowes). *Bd*-infected frogs are expected to be more prevalent when water is available because the fungus has an aquatic zoospore that takes around five days to complete its life cycle (Berger *et al.* 2005; Van Rooij *et al.* 2015). However, identifying the mortality threshold and associated level of infection is difficult in the field. We have quantified 10^{10} *Bd* ITS copies from individuals in natural populations (unpublished data, Longo & Burrowes), and moribund individuals have been reported with a level of infection as low as 10^4 and 10^5 zoospores (Longo *et al.* 2013). Finally, infection with *Bd* is more common in smaller-sized adults in nature (Burrowes *et al.* 2008), suggesting infected direct-developing frogs incur a tradeoff between growth and immune response.

Table 1: Description of parameters used in the models and associated values.

Parameter	Description	Values
t	Current time steps reflecting an increase of one week each for one year. One year corresponds to species growing season —hatching to maturity—.	{1:52} for weeks 1:52
$t+1$	Indicates the next time step.	{2:52} for weeks 2:52
S	Size states, each reflecting an increase of 0.44 mm in juveniles and 0.22 mm in adults SVL (snout-to-vent length) based on species pre- and post-maturity sizes.	{1:208}, where - juveniles {1:50} for 6:28mm - adults {51:208} for 28:63mm
I	Level of infection reflecting a ten-fold increase in the number of *Bd*-zoospores as a measure of the pathogen burden.	{0:10}, where - 0 = non-infected - {1:10} = ($10^1 : 10^{10}$) zoospores
i	Strategies to allocate their available energy each week.	$\{G, C, B\}$ where - G = Grow - C = Control infection - B = Grow /control infection
E	Weekly energy units obtained from foraging based on probability as a function of the model and season.	{0, 2, 4} with a probability of: - {0.33, 0.33, 033} in No seasons - {0.45, 0.45, 0.1} in Cool season - {0.1, 0.45, 0.45} in Warm season
P_I	Probability of an uninfected individual becoming infected based on the prevalence of the pathogen in nature.	- No season = 0.45 - Cool = 0.51 - Warm = 0.39
$M_S(S)$	Probability of dying due to causes other than the infection estimated as a function of size.	Defined in equation 3
d	Decreasing constant rate of the probability of dying as a function of size.	0.05
S_T	Constant indicating the size at the mid probability of dying using the maturity size state $S = 50$.	50
M_I	Probability of dying due to the level of infection, the value increases one-fold every two levels of infection.	{0:10^{-1}}, where - $MI_0 = 0$, $MI_{1:2} = 9 * 10^{-5}$, - $MI_{3:4} = 9 * 10^{-4}$ - $MI_{5:6} = 9 * 10^{-3}$, - $MI_{7:8} = 9 * 10^{-2}$ - $MI_{9:10} = 9 * 10^{-1}$

Figure legends

Figure 1. Diagram illustrating: (**a**) the expected growth rates at different life stages and (**b**) the grow-defense tradeoff hypotheses during the time horizon examined using dynamic optimization models based on the *E. coqui* and *Bd* system in Box 1. In **a**, juveniles grow at a constant rate independently of sex, growth rate decreases after maturity, and it can vary between sexes. Because we focused on the development of juveniles, we used the mean growth rate (dashed line). The growth rate graph was adapted for *E. coqui* from Joglar (1998). In **b**, differences in prey diversity and abundance between seasons determine energy intake, and the difference in pathogen spreading capacity influences the probability of an uninfected individual to become infected. Whereas, the infection status affects energy allocation towards growth or pathogen defense. As a result, growth rate will be higher when individuals allocate all their energy to grow, thus reaching maturity earlier. The arrows' width is proportional to the amount of energy intake allocated to each process. Words in grey indicate no energy allocated to the process, and the relative size of the frogs illustrates growth rates.

Figure 2. Decision matrices for different infection levels and seasonal scenarios. Our models include the basic model (**a**) and different seasonal scenarios (**b-d**) in which the cool (C) and warm (W) periods are alternated. The cool season was characterized for individuals less energy available (E in equation 1) and a lower probability of getting infected (P_I in equation 7) than in the warm season. Colors indicate the best strategies to increase future fitness generated by the model. Each graph's size states increase from the bottom to the top (0-208) and time from left to right (1-52 wks). For the level of infection, 0 indicates uninfected, and 1 to 10 corresponds to 10^1 to 10^{10} *Bd* zoospores. Each panel corresponds to a specific level of infection for each model-scenario combination. Parameter values of these models were based on the *E. coqui* and *Bd* system in Box 1.

Figure 3. Growth of the individuas (size in snout-to-vent length, SVL) based on the forward simulations (**a**) and the relationship between growth rate and mean level of infection (**b**) based

on optimized strategies for one simulation with 100 individuals inferred by the basic (**top**) and seasonal models. Parameter values change based on the model and seasonal scenarios in which the cool (C) and warm (W) seasons are alternated. The cool season was characterized for individuals less energy available (E in equation 1) and a lower probability of getting infected (P_I in equation 7) than in the warm season. Each line in (**a**) represents one single frog, the colors indicate the level of infection at each time step, and the (x) shows when the individual died. Vertical grey lines separate the year into four periods of 13 weeks, which in the seasonal model correspond to a specific season; dashed-horizontal lines indicate the size state at which individuals reach maturity (S=50). Solid black lines track the mean growth rate trend for each simulation. Each point in **b** represents a period of 13 weeks for each individual. Parameter values of these models were based on the *E. coqui* and *Bd* system in Box 1.

Figure 4. Fitness-related values distributions for the *basic* (No seasons) and the *seasonality* models including: (**a**) the number of individuals that reached maturity within one year, (**b**) mean time to maturity, (**c**) mean size at week 52, and (**c**) percentage of individuals surviving in week 52. Data distributions correspond to 100 forward simulations of the dynamic optimization models with 100 individuals per simulation for the base and seasonality models, including seasonal alternations between cool (C) and warm (W) periods. The cool season was characterized by less energy available (E in equation 1) and a lower probability of getting infected (P_I in equation 7) than in the warm season.

Figure 5. Population dynamics for the *basic* (No seasons) and the *seasonality* models including: (**a**) Number of individuals that were susceptible (S), infected (I), and removed (R) and (**b**) mean *Bd* zoospores of the population across time. Data corresponds to 100 forward simulations of the dynamic optimization models with 100 individuals per simulation for the base and seasonality models, including seasonal alternations between cool (C) and warm (W) periods. The cool season was characterized by less energy available (E in equation 1) and a lower probability of getting infected (P_I in equation 7) than in the warm season.

Figure S1. Probability of dying as a function of discrete (**a**) size–S and (**b**) infection–I states based on equations 3 and 4, respectively. Although the equations are the same, parameter values are indicated by colors. In (**a**), we varied the probability of dying as a function in one year at the smallest size state (M_H), whereas in (**b**), the probability of dying at the highest infection level ($M_I(I = 10)$). Note they are in a log_{10} scale.

Figure S2. Forward simulations (**a-e**) based on optimized strategies for 100 individuals inferred by the *basic* (No seasons) (**a**) and *seasonal* (**b-e**) models using the size of the individuals (snout-to-vent length – SVL) instead of the size states of the model. We calculated size based on the following formulas: for size states $\geq 50[(S-1)*0.44+6]$ and for size states $> 50[6+(49*0.44)+(S-50)*0.22)]$. Parameter values change based on the model and seasonal scenarios in which the cool (C) and warm (W) seasons are alternated. The cool season was characterized by less energy available (E in equation 1) and a lower probability of getting infected (P_I in equation 7) than in the warm season. Each line represents one single frog, the colors indicate the level of infection at each time step, and the (x) shows when the individual died. Vertical grey lines separate the year into four periods of 13 weeks, which in the seasonal model correspond to a specific season; dashed-horizontal lines indicate the size state at which individuals reach maturity (SVL=28).

Figure S3. Prevalence of *Bd*-infected individuals at Palo Colorado Forest in El Yunque, Puerto Rico. Prevalence was calculated by monthly sampling for over a year (unpublished data, Longo & Burrowes).

Figure S4. Growth of the individuals (size states) based on the forward simulations (**a**) and the relationship between growth rate and mean level of infection (**b**) based on optimized strategies for one simulation with 100 individuals inferred by the basic (**top**) and seasonal models. Parameter values change based on the model and seasonal scenarios in which the cool (C) and warm (W) seasons are alternated. The cool season was characterized for individuals less energy available (E in equation 1) and a lower probability of getting infected (P_I in equation 7)

than in the warm season. Each line in (**a**) represents one single frog, the colors indicate the level of infection at each time step, and the (x) shows when the individual died. Vertical grey lines separate the year into four periods of 13 weeks, which in the seasonal model correspond to a specific season; dashed-horizontal lines indicate the size state at which individuals reach maturity (S=50). Solid black lines track the mean growth rate trend for each simulation. Each point in **b** represents a period of 13 weeks for each individual. Parameter values of these models were based on the *E. coqui* and *Bd* system in Box 1.

Figure S5. Fitness-related value distributions associated with maturity variables for the *basic* (No seasons) and the *seasonality* models, in which the cool (C) and warm (W) seasons are alternated. The cool season was characterized for individuals less energy available (E in equation 1) and a lower probability of getting infected (P_I in equation 7) than in the warm season. Fitness traits included: (**a**) the number of individuals that reached maturity within one year and (**b**) mean time to maturity. Data distributions correspond to 100 forward simulations of the dynamic optimization models with 100 individuals per simulation for each one of the combinations in parameter values. In the models id codes, S indicates the probability of dying as function of size (M_S), where in S2 $M_H = 0.2$, in S4 $M_H = 0.4$, in S6 $M_H = 0.6$, and in S8 $M_H = 0.8$ using equation 3 (see Fig. S1a); and D indicates the probability of dying due to the infection level (M_I), where in D1 ranged from 1×10^{-5} to 1×10^{-1}, in D5 ranged from 5×10^{-5} to 5×10^{-1}, in D9 ranged from 9×10^{-5} to 9×10^{-1}, and in D10 ranged from 9×10^{-4} to 1×10^{0} following equation 4 (see Fig. S1b). S8D9 corresponds to the original model based on *E. coqui* - *Bd* study system (Box1).

Figure S6. Fitness-related value distributions associated with the end of the time horizon variables for the *basic* (No seasons) and the *seasonality* models, in which the cool (C) and warm (W) seasons are alternated. The cool season was characterized for individuals less energy available (E in equation 1) and a lower probability of getting infected (P_I in equation 7) than in the warm season. Fitness traits included: (**a** mean size at week 52, and (**b**) percentage

of individuals surviving in week 52. Data distributions correspond to 100 forward simulations of the dynamic optimization models with 100 individuals per simulation for each one of the combinations in parameter values. In the models id codes, S indicates the probability of dying as function of size (M_S), where in S2 $M_H = 0.2$, in S4 $M_H = 0.4$, in S6 $M_H = 0.6$, and in S8 $M_H = 0.8$ using equation 3 (see Fig. S1a); and D indicates the probability of dying due to the infection level (M_I), where in D1 ranged from 1×10^{-5} to 1×10^{-1}, in D5 ranged from 5×10^{-5} to 5×10^{-1}, in D9 ranged from 9×10^{-5} to 9×10^{-1}, and in D10 ranged from 9×10^{-4} to 1×10^{0} following equation 4 (see Fig. S1b). S8D9 corresponds to the original model based on *E. coqui - Bd* study system (Box1).

Figure 1:

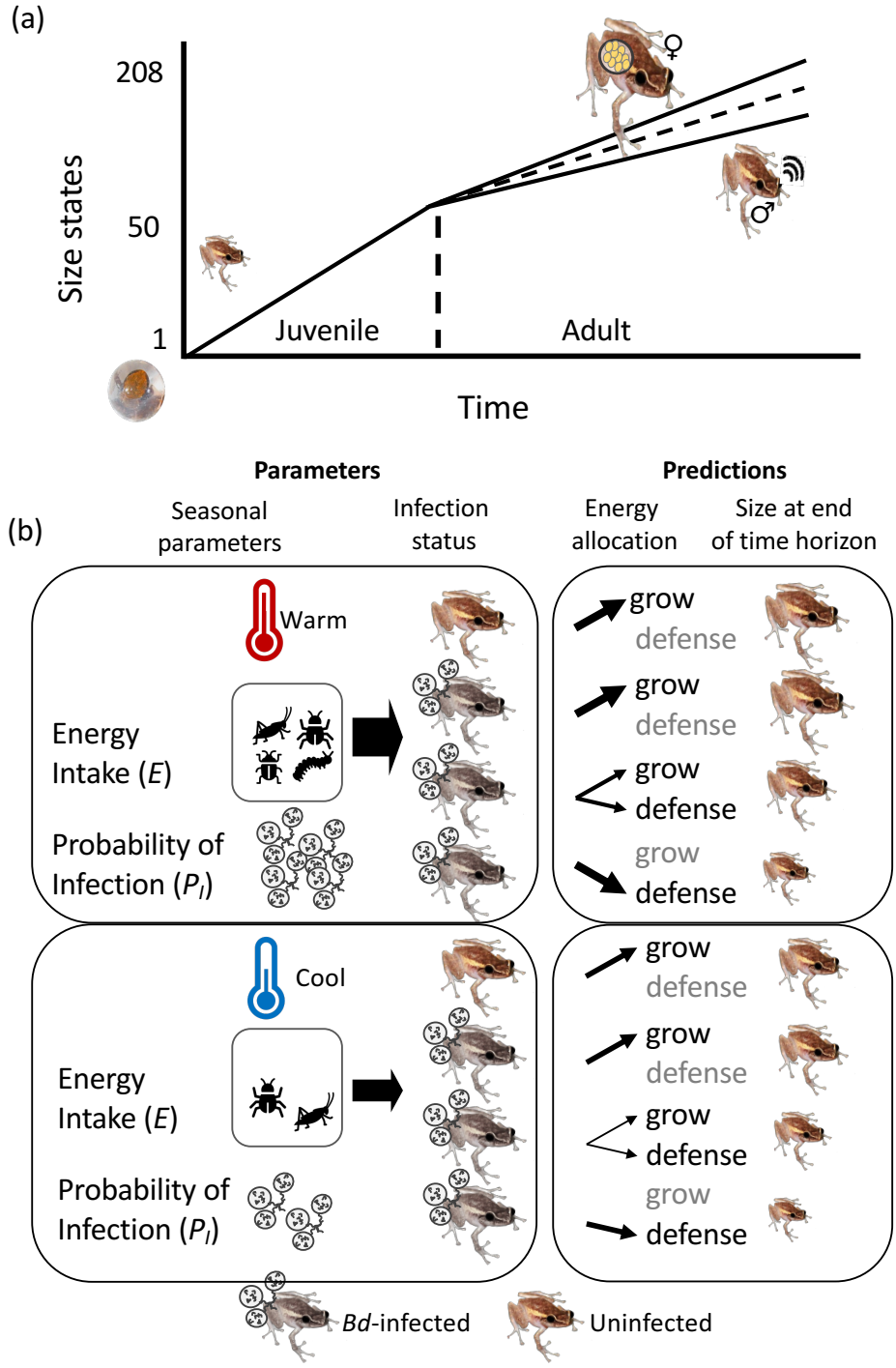
(a)
208
50
1
Size states
Juvenile
Adult
Time
♀
♂
(b)
Parameters
Predictions
Seasonal parameters
Infection status
Energy allocation
Size at end of time horizon
Warm
Energy Intake (E)
Probability of Infection (P_I)
grow
defense
grow
defense
grow
defense
grow
defense
Cool
Energy Intake (E)
Probability of Infection (P_I)
grow
defense
grow
defense
grow
defense
grow
defense
Bd-infected
Uninfected

Figure 2:

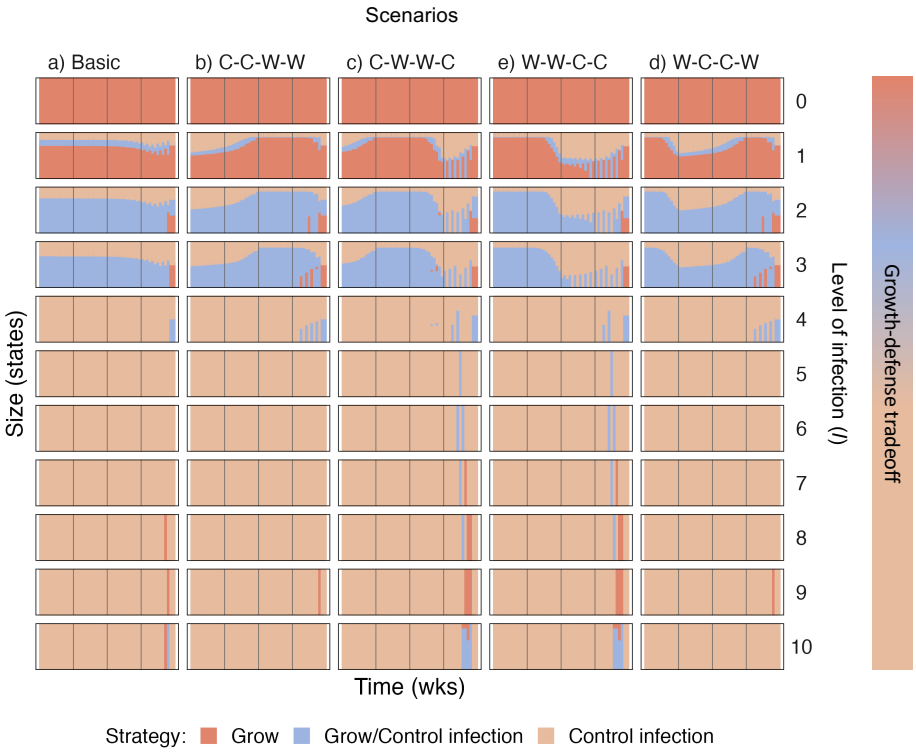
Scenarios
a) Basic
b) C-C-W-W
c) C-W-W-C
e) W-W-C-C
d) W-C-C-W
Size (states)
Time (wks)
Level of infection (I)
0
1
2
3
4
5
6
7
8
9
10
Growth-defense tradeoff
Strategy:
Grow
Grow/Control infection
Control infection

Figure 3:

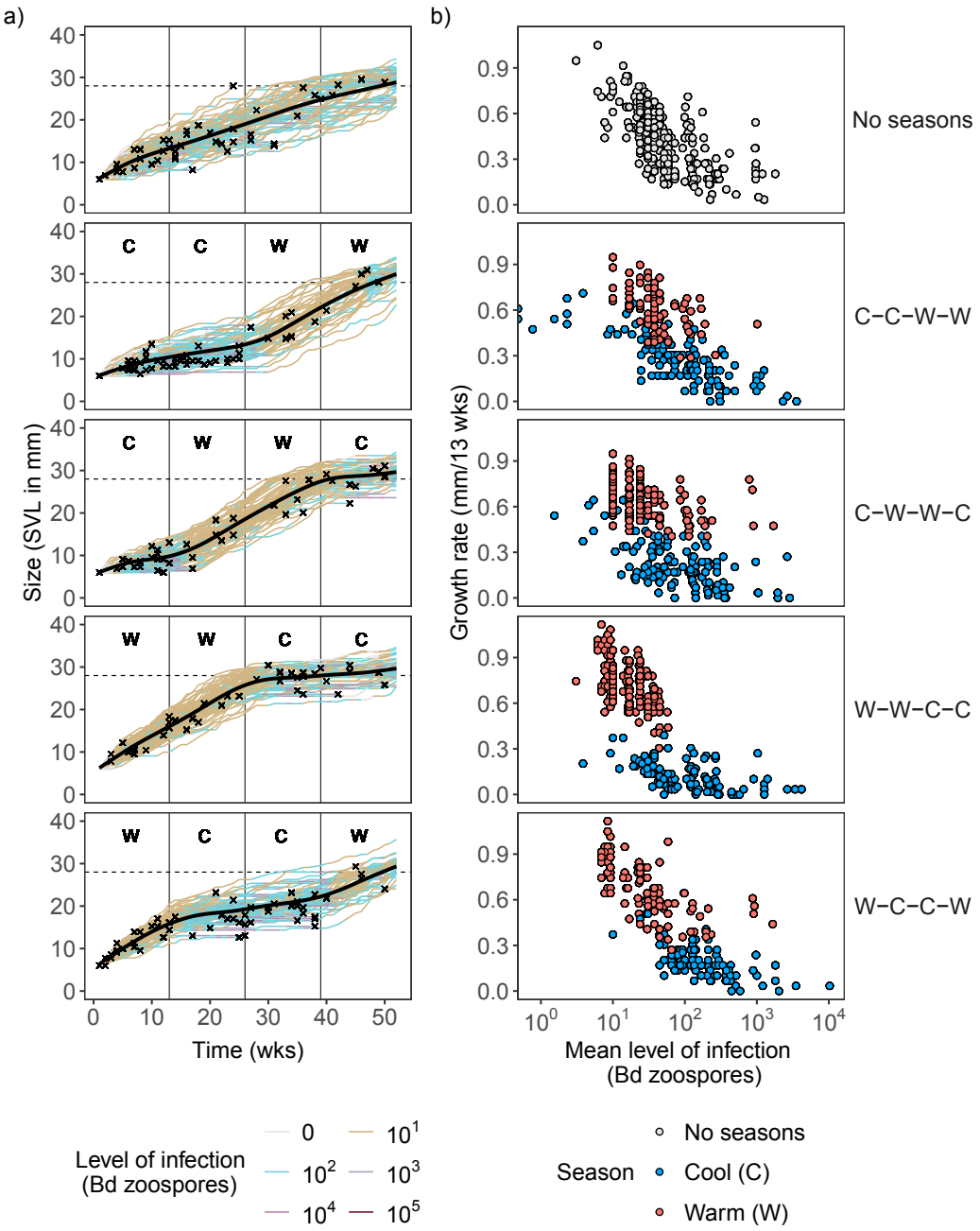
a)
b)
Size (SVL in mm)
Time (wks)
C C W W
C W W C
W W C C
W C C W
Growth rate (mm/13 wks)
Mean level of infection
(Bd zoospores)
No seasons
C−C−W−W
C−W−W−C
W−W−C−C
W−C−C−W
Level of infection
(Bd zoospores)
0
10^1
10^2
10^3
10^4
10^5
Season
No seasons
Cool (C)
Warm (W)

Figure 4:

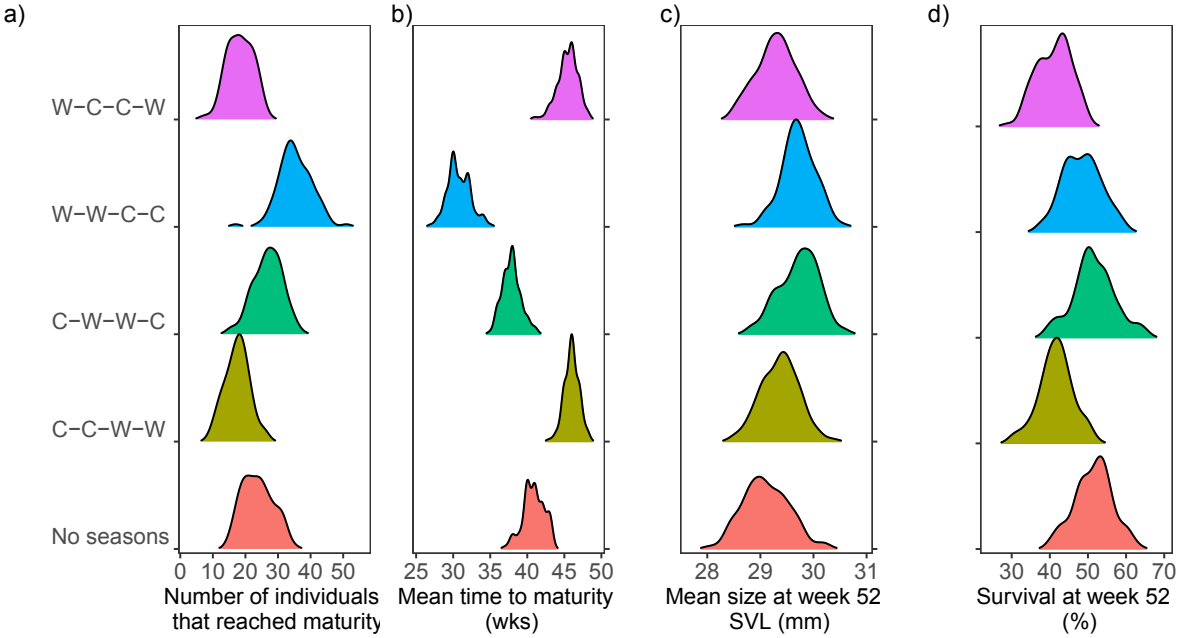
a)
b)
c)
d)
W−C−C−W
W−W−C−C
C−W−W−C
C−C−W−W
No seasons
0 10 20 30 40 50
Number of individuals that reached maturity
25 30 35 40 45 50
Mean time to maturity (wks)
28 29 30 31
Mean size at week 52 SVL (mm)
30 40 50 60 70
Survival at week 52 (%)

Figure 5:

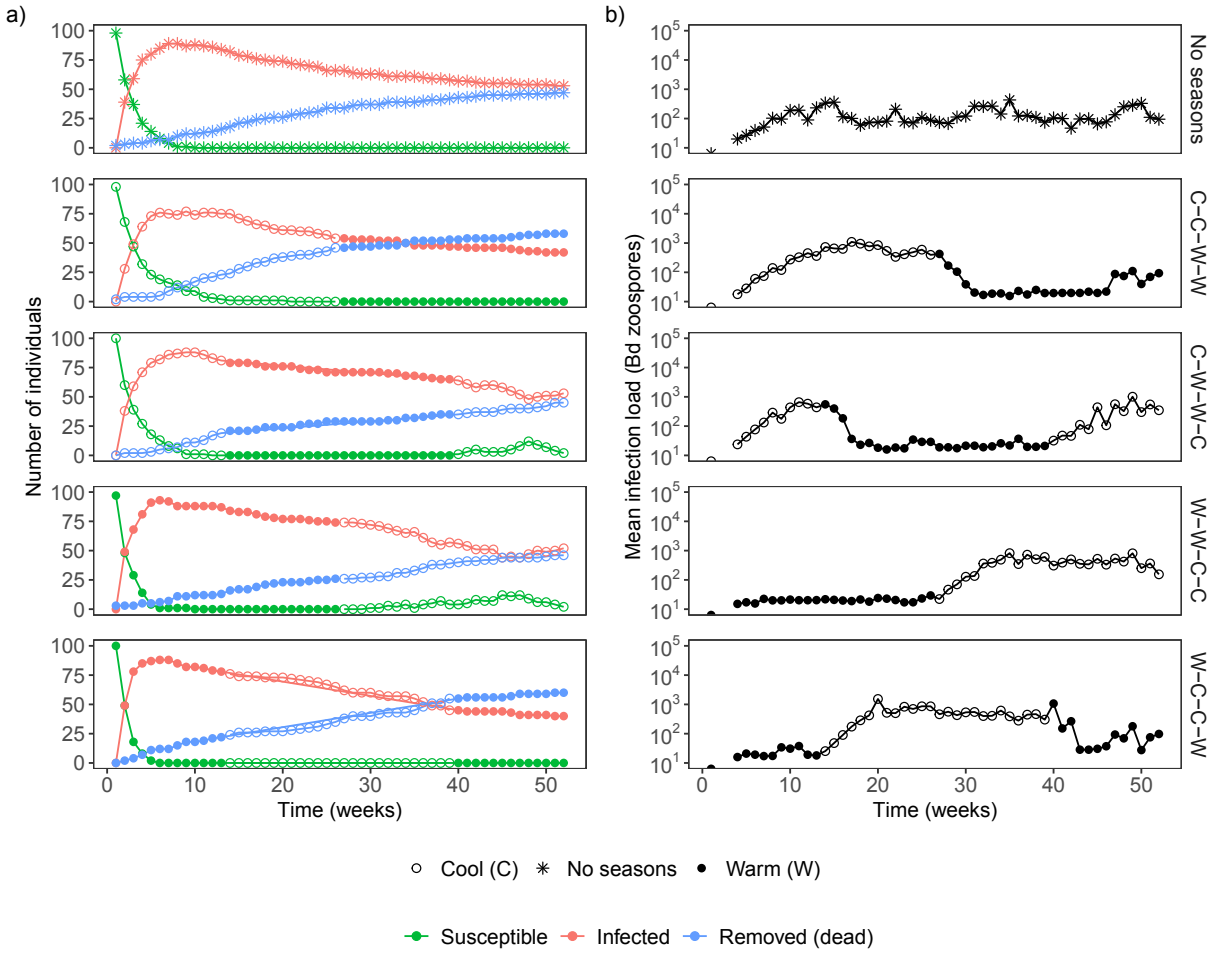
a)
b)
Number of individuals
Mean infection load (Bd zoospores)
Time (weeks)
Time (weeks)
No seasons
C–C–W–W
C–W–W–C
W–W–C–C
W–C–C–W
Cool (C)
No seasons
Warm (W)
Susceptible
Infected
Removed (dead)

Figure S1:

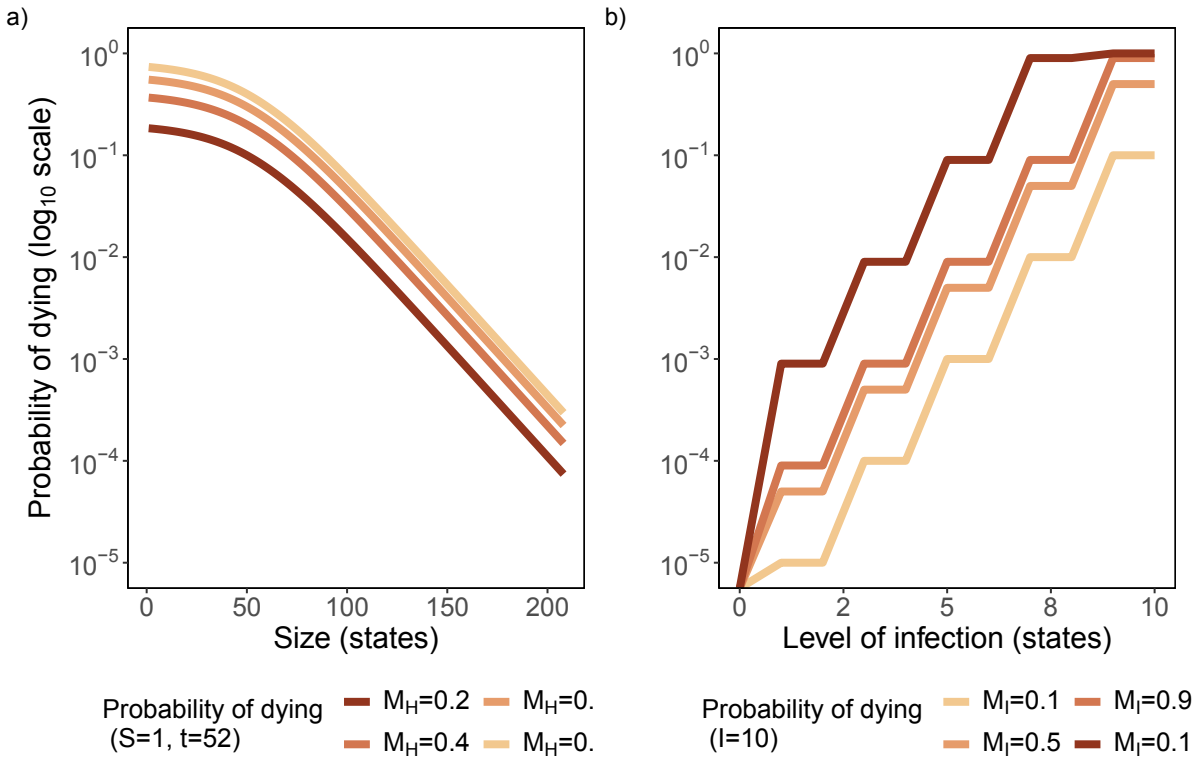
a)
b)
Probability of dying (log10 scale)
Size (states)
Level of infection (states)
Probability of dying
(S=1, t=52)
MH=0.2
MH=0.
MH=0.4
MH=0.
Probability of dying
(I=10)
MI=0.1
MI=0.9
MI=0.5
MI=0.1

Figure S2:

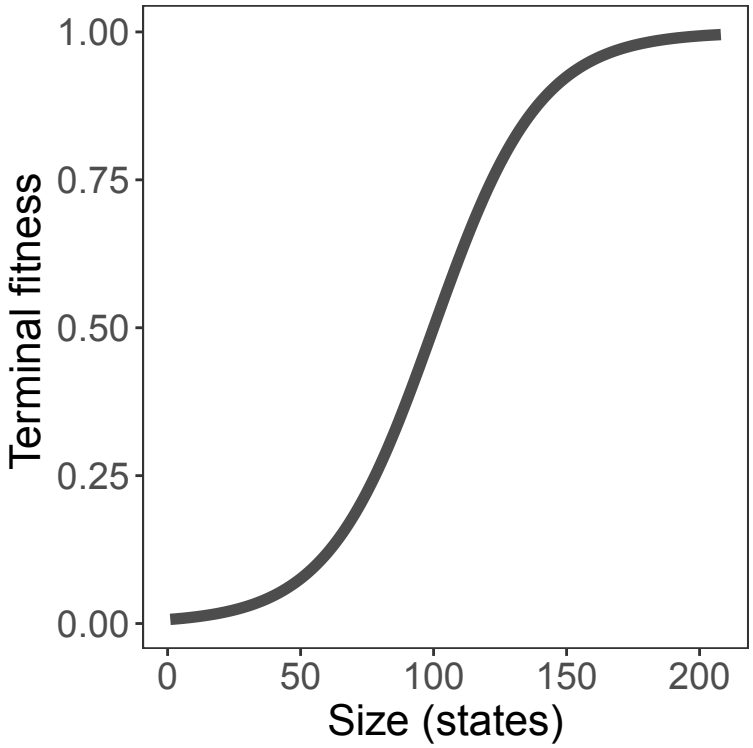
1.00
0.75
0.50
0.25
0.00
Terminal fitness
0
50
100
150
200
Size (states)

Figure S3:

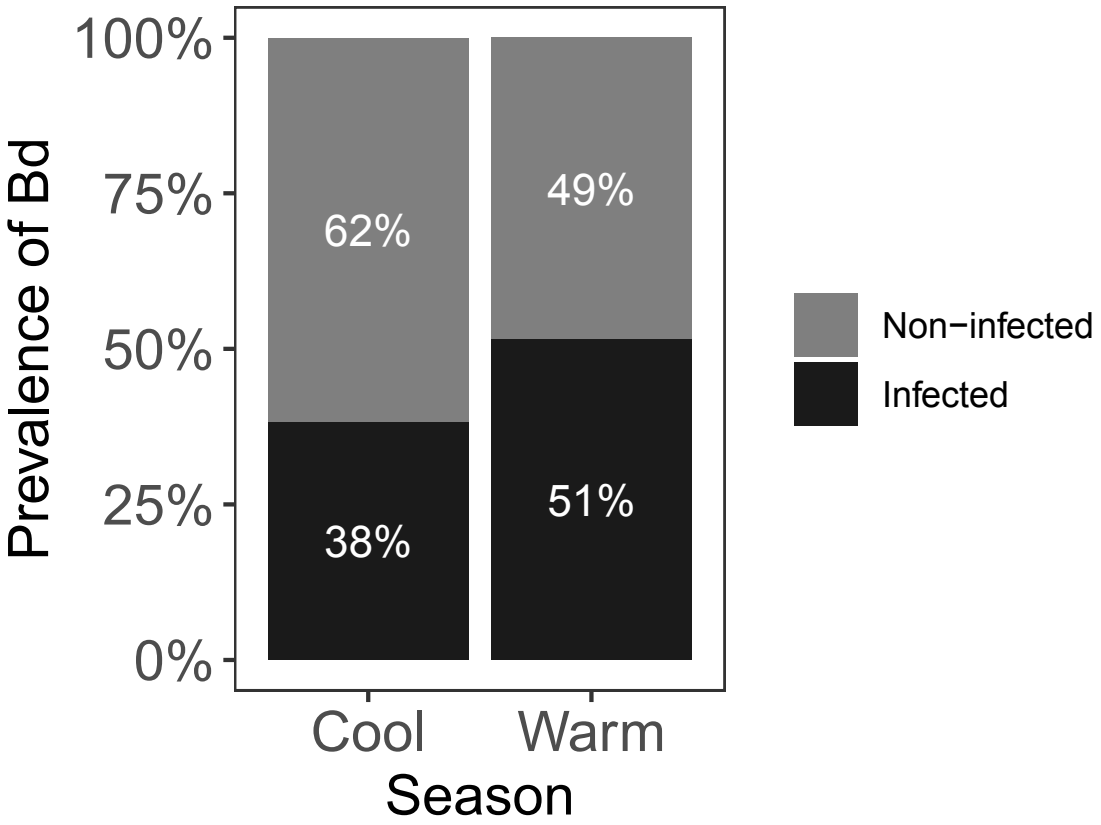
100%
75%
50%
25%
0%
Prevalence of Bd
62%
38%
49%
51%
Cool
Warm
Season
Non−infected
Infected

Figure S4:

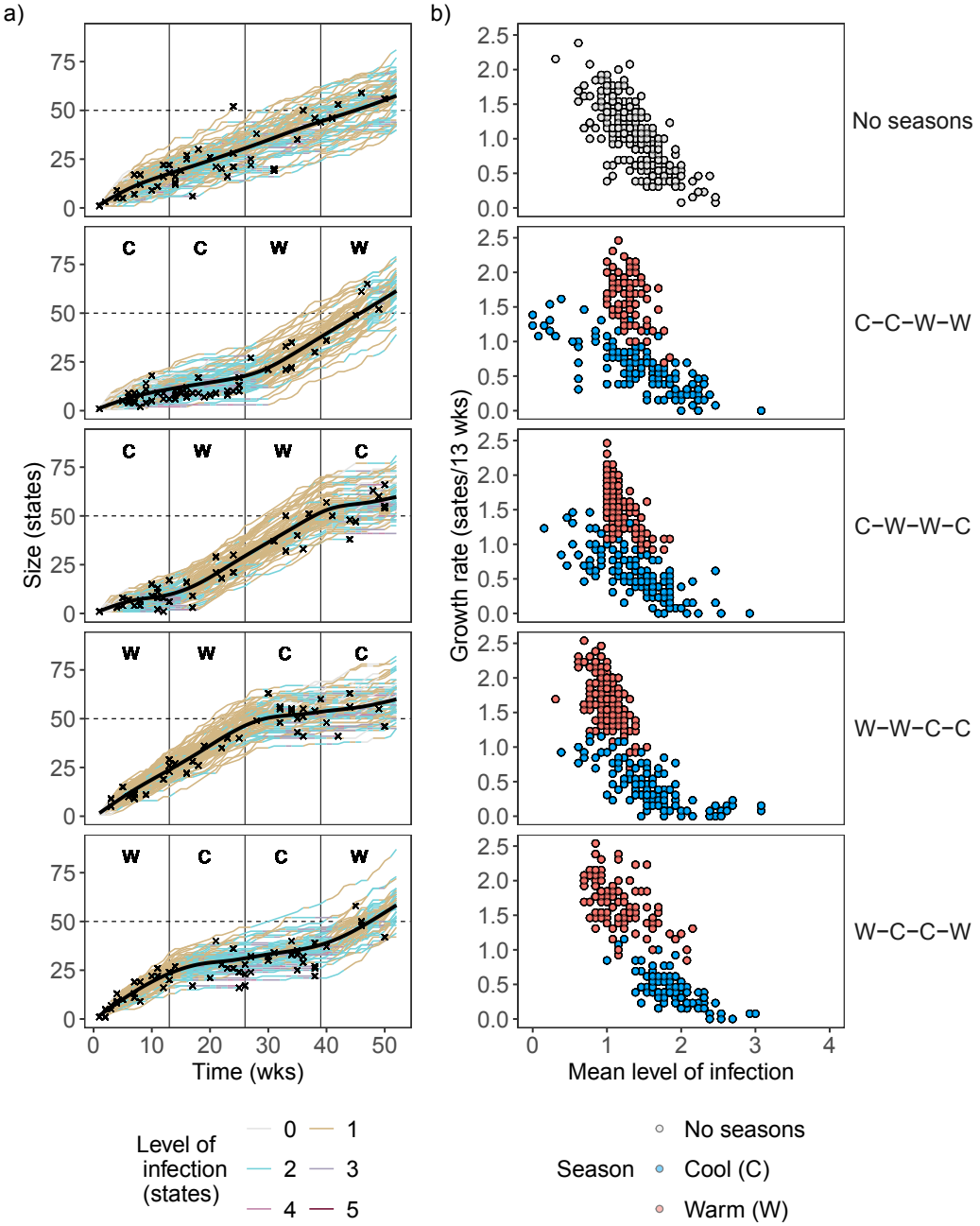
a)
b)
Size (states)
Time (wks)
Growth rate (sates/13 wks)
Mean level of infection
No seasons
C−C−W−W
C−W−W−C
W−W−C−C
W−C−C−W
Level of infection (states)
0
1
2
3
4
5
Season
No seasons
Cool (C)
Warm (W)

Figure S5:

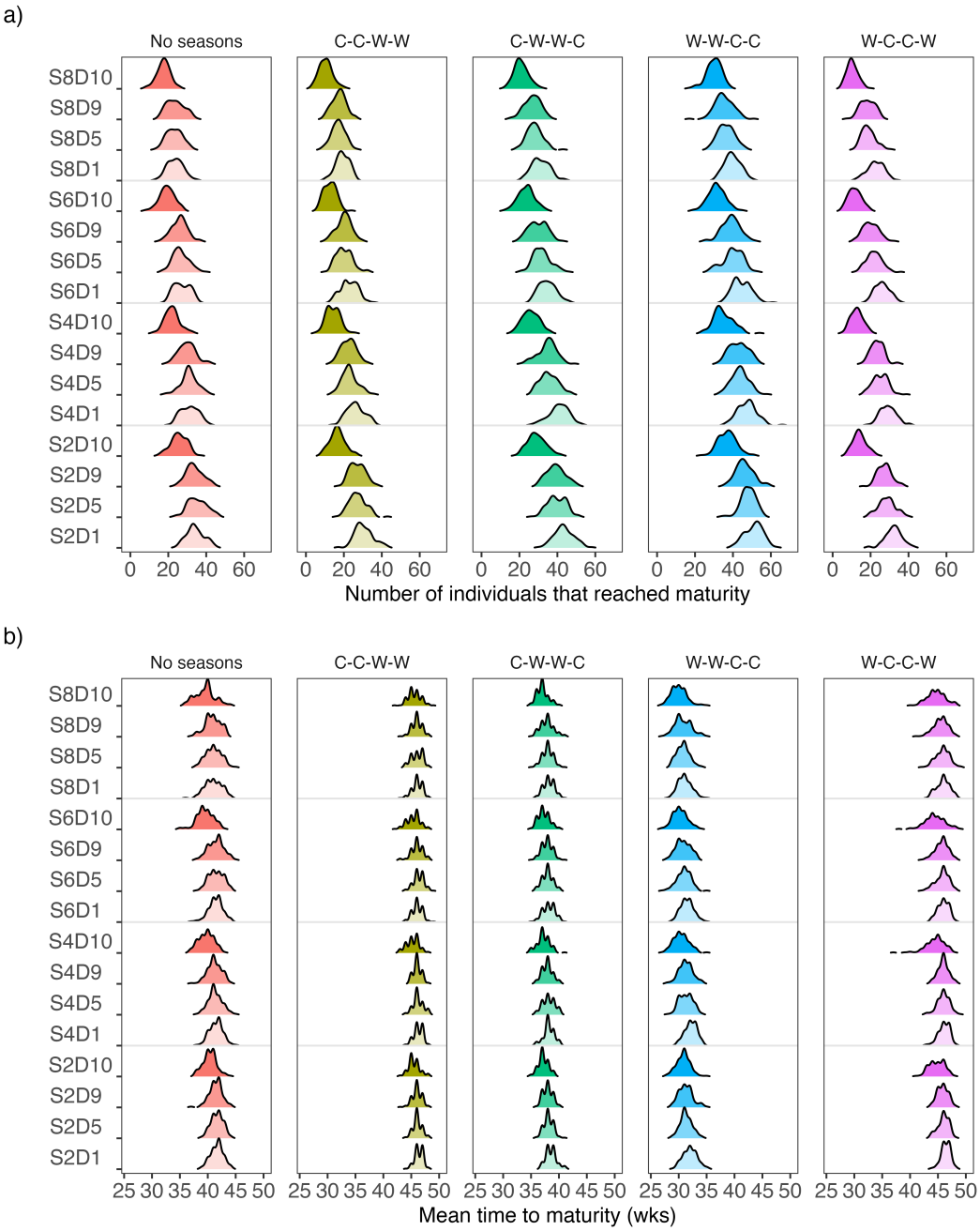
a)
No seasons
C-C-W-W
C-W-W-C
W-W-C-C
W-C-C-W
S8D10
S8D9
S8D5
S8D1
S6D10
S6D9
S6D5
S6D1
S4D10
S4D9
S4D5
S4D1
S2D10
S2D9
S2D5
S2D1
0 20 40 60
Number of individuals that reached maturity
b)
25 30 35 40 45 50
Mean time to maturity (wks)

Figure S6:

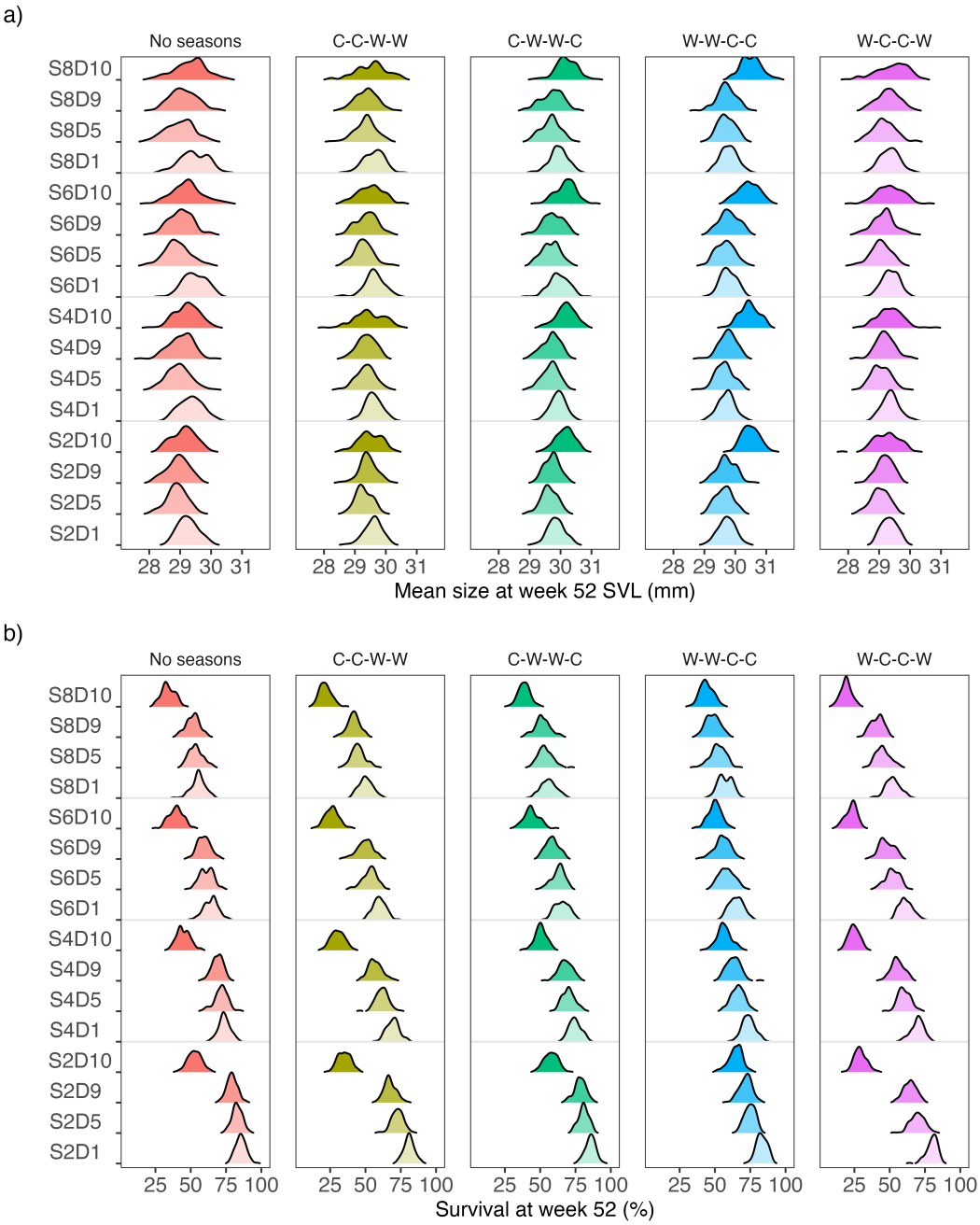
a)
No seasons
C-C-W-W
C-W-W-C
W-W-C-C
W-C-C-W
S8D10
S8D9
S8D5
S8D1
S6D10
S6D9
S6D5
S6D1
S4D10
S4D9
S4D5
S4D1
S2D10
S2D9
S2D5
S2D1
28 29 30 31
Mean size at week 52 SVL (mm)
b)
25 50 75 100
Survival at week 52 (%)